

1 **Neurotrophic factor Neuritin modulates T cell electrical and metabolic state for the balance**  
2 **of tolerance and immunity**

3  
4 Hong Yu<sup>1,2\*#</sup>, Hiroshi Nishio<sup>1, 2, 3, #</sup>, Joseph Barbi<sup>1,2,4, #</sup>, Marisa Mitchell-Flack<sup>1,2</sup>, Paolo D. A.  
5 Vignali<sup>1,2,5</sup>, Ying Zheng<sup>1, 2</sup>, Andriana Lebid<sup>1,2</sup>, Kwang-Yu Chang<sup>1,6</sup>, Juan Fu<sup>1,2</sup>, Makenzie  
6 Higgins<sup>1</sup>, Ching-Tai Huang<sup>2, 7</sup>, Xuehong Zhang<sup>8</sup>, Zhiguang Li<sup>8</sup>, Lee Blosser<sup>1</sup>, Ada Tam<sup>1</sup>, Charles  
7 G. Drake<sup>2,9</sup>, and Drew M. Pardoll<sup>1,2</sup>

8  
9 <sup>1</sup> Bloomberg-Kimmel Institute for Cancer Immunotherapy, Immunology and Hematopoiesis  
10 Division, Department of Oncology, Johns Hopkins University School of  
11 Medicine, Baltimore, Maryland.

12 <sup>2</sup> The Sidney Kimmel Comprehensive Cancer Center, Johns Hopkins University School of  
13 Medicine, Baltimore, Maryland.

14 <sup>3</sup> Current address: Department of Obstetrics and Gynecology, Keio University School of  
15 Medicine, Tokyo 160-8582, Japan

16 <sup>4</sup> Current address: Department of Immunology, Roswell Park Comprehensive Cancer Center,  
17 Buffalo, NY14263, USA

18 <sup>5</sup> Current address: University of Pittsburgh, Carnegie Mellon.

19 <sup>6</sup> Current address: National Institute of Cancer Research, National Health Research Institutes,  
20 Tainan, Taiwan

21 <sup>7</sup> Current address: Infectious Diseases, Department of Medicine, Chang Gung Memorial  
22 Hospital, Taiwan

23 <sup>8</sup> Institute of Cancer Stem Cell, Cancer Center, Dalian Medical University, Dalian 116044,  
24 China.

25 <sup>9</sup>Current address: Division of Hematology and Oncology, Herbert Irving Comprehensive Cancer  
26 Center, Columbia University Medical Center, New York, New York 10032.

27 # These authors contributed equally to this work.

28 \*Correspondence to [hyu13@jhmi.edu](mailto:hyu13@jhmi.edu).

29

30

31

32

33

34

35

36

37

38

39

40 **Abstract:**

41 The adaptive T cell response is accompanied by continuous rewiring of the T cell's electric and  
42 metabolic state. Ion channels and nutrient transporters integrate bioelectric and biochemical  
43 signals from the environment, setting cellular electric and metabolic states. Divergent electric and  
44 metabolic states contribute to T cell immunity or tolerance. Here, we report that neuritin (Nrn1)  
45 contributes to tolerance development by modulating regulatory and effector T cell function. Nrn1  
46 expression in regulatory T cells promotes its expansion and suppression function, while expression  
47 in the T effector cell dampens its inflammatory response. Nrn1 deficiency causes dysregulation  
48 of ion channel and nutrient transporter expression in Treg and effector T cells, resulting in  
49 divergent metabolic outcomes and impacting autoimmune disease progression and recovery.  
50 These findings identify a novel immune function of the neurotrophic factor Nrn1 in regulating the  
51 T cell metabolic state in a cell context-dependent manner and modulating the outcome of an  
52 immune response.

53

54

55

56

57

58

59

60

61

62

63

64

65

66

67

68

69

70

## 71 **Introduction**

72           Peripheral T cell tolerance is important in restricting autoimmunity and minimizing  
73 collateral damage during active immune reactions and is achieved via diverse mechanisms,  
74 including T cell anergy, regulatory T (Treg) cell mediated suppression, and effector T (Te) cell  
75 exhaustion or deletion (ElTanbouly and Noelle, 2021). Upon activation, Treg and conventional T  
76 cells integrate environmental cues and adapt their metabolism to the energetic and biosynthetic  
77 demands, leading to tolerance or immunity. Tolerized versus responsive T cells are characterized  
78 by differential metabolic states. For example, T cell anergy is associated with reduced glycolysis,  
79 whereas activated T effector cells exhibit increased glycolysis (Buck et al., 2017; Geltink et al.,  
80 2018; Peng and Li, 2023; Zheng et al., 2009). Cellular metabolic states depend on electrolyte and  
81 nutrient uptake from the microenvironment (Chapman and Chi, 2022; Olenchok et al., 2017). Ion  
82 channels and nutrient transporters, which can integrate environmental nutrient changes, affect the  
83 cellular metabolic choices and impact the T cell functional outcome (Babst, 2020; Bohmwald et  
84 al., 2021; Ramirez et al., 2018). Each cell's functional state would correspond with a set of ion  
85 channels and nutrient transporters supporting their underlying metabolic requirements. The  
86 mechanisms coordinating the ion channel and nutrient transporter expression changes to support  
87 the adaptive T cell functional state in the immune response microenvironment remain unclear.

88           Nrn1, also known as candidate plasticity gene 15 (CPG15), was initially discovered as a  
89 neurotrophic factor linked to the neuronal cell membrane through a glycosylphosphatidylinositol  
90 (GPI) anchor (Nedivi et al., 1998; Zhou and Zhou, 2014). It is highly conserved across species,  
91 with 98% overall homology between the murine and human protein. Nrn1 plays multiple roles in  
92 neural development, synaptic plasticity, synaptic maturation, neuronal migration, and survival  
93 (Cantalops et al., 2000; Javaherian and Cline, 2005; Nedivi et al., 1998; Putz et al., 2005; Zito et  
94 al., 2014). In the immune system, Nrn1 expression has been found in Foxp3<sup>+</sup> Treg and follicular  
95 regulatory T cells (Tfr) (Gonzalez-Figueroa et al., 2021; Vahl et al., 2014), T cells from transplant  
96 tolerant recipients (Lim et al., 2013), anergized CD8 cells or CD8 cells from tumor-infiltrating  
97 lymphocytes in mouse tumor models (Schietinger et al., 2012; Schietinger et al., 2016; Singer et  
98 al., 2016), and in human Treg infiltrating breast cancer tumor tissue (Plitas et al., 2016). Soluble  
99 Nrn1 can be released from Tfr cells and act directly on B cells to suppress autoantibody  
100 development against tissue-specific antigens (Gonzalez-Figueroa et al., 2021). Despite the  
101 observation of Nrn1 expression in Treg cells and T cells from tolerant environments (Gonzalez-

102 Figueroa et al., 2021; Lim et al., 2013; Plitas et al., 2016; Schietinger et al., 2012; Schietinger et  
103 al., 2016; Singer et al., 2016), the roles of *Nrn1* in T cell tolerance development and Treg cell  
104 function have not been explored, and functional mechanism of *Nrn1* remains elusive. This study  
105 demonstrates that the neurotrophic factor *Nrn1* can moderate T cell tolerance and immunity  
106 through both Treg and Te cells, impacting Treg cell expansion and suppression while controlling  
107 inflammatory response in Te cells.

108

## 109 **Results**

### 110 ***Nrn1* expression and function in T cell anergy.**

111 To explore the molecular mechanisms underlying peripheral tolerance development, we  
112 utilized a system we previously developed to identify tolerance-associated genes (Huang et al.,  
113 2004). We compared the gene expression patterns associated with either a T effector/memory  
114 response or tolerance induction triggered by the same antigen but under divergent *in vivo*  
115 conditions (Huang et al., 2004). Influenza hemagglutinin (HA) antigen-specific TCR transgenic  
116 CD4 T cells were adoptively transferred into WT recipients with subsequent HA-Vaccinia virus  
117 (VacHA) infection to generate T effector/memory cells while tolerogenic HA-specific CD4s were  
118 generated by transfer into hosts with transgenic expression of HA as self-antigen (C3-HA mice,  
119 Figure 1A.)(Huang et al., 2004). One of the most differentially expressed genes upregulated in the  
120 anergy-inducing condition was *Nrn1*. *Nrn1* expression was significantly higher among cells  
121 recovered from C3-HA hosts vs. cells from VacHA infected mice at all time points tested by qRT-  
122 PCR (Figure 1A). To further confirm the association of *Nrn1* expression with T cell anergy, we  
123 assessed *Nrn1* expression in naturally occurring anergic polyclonal CD4<sup>+</sup> T cells (Ta), which can  
124 be identified by surface co-expression of Folate Receptor 4 (FR4) and the ecto-5'-nucleotidase  
125 CD73 (Ta, CD4<sup>+</sup>CD44<sup>+</sup>FR4<sup>hi</sup>CD73<sup>hi</sup> cells)(Kalekar et al., 2016). *Nrn1* expression was  
126 significantly higher in Ta than in naïve CD4 (Tn, CD4<sup>+</sup>CD62L<sup>+</sup>CD44<sup>-</sup>FR4<sup>-</sup>CD73<sup>-</sup>) and antigen-  
127 experienced cells (Te, CD4<sup>+</sup>CD44<sup>+</sup>FR4<sup>-</sup>CD73<sup>-</sup>) under steady-state conditions measured by both  
128 qRT-PCR and western blot (Figure 1B). Given that Treg cells, like anergic cells, have roles in  
129 maintaining immune tolerance, we queried whether *Nrn1* is also expressed in Treg cells. *Nrn1*  
130 expression can be detected in nTreg and induced Treg (iTreg) cells generated *in vitro* (Figure 1C).

131 To evaluate *Nrn1* expression under pathological tolerant conditions (Cuenca et al., 2003),  
132 we evaluated *Nrn1* expression in T cells within the tumor microenvironment. *Nrn1* expression in

133 murine Treg cells and non-Treg CD4<sup>+</sup> cells from tumor infiltrates were compared to the Treg cells  
134 and non-Treg CD4<sup>+</sup> T cells isolated from peripheral blood. Nrn1 mRNA level was significantly  
135 increased among tumor-associated Treg cells and non-Treg CD4 cells compared to cells from  
136 peripheral blood (Figure 1-figure supplement 1A). Consistent with our findings in the mouse tumor  
137 setting, the Treg and non-Treg T cells from human breast cancer infiltrates reveal significantly  
138 higher Nrn1 expression compared to the peripheral blood Treg and non-Treg cells (Figure 1-figure  
139 supplement 1B) (Plitas et al., 2016).

140 CD4<sup>+</sup> T cells may pass through an effector stage after activation before reaching an anergic  
141 state (Adler et al., 1998; Chen et al., 2004; Huang et al., 2003; Opejin et al., 2020). To evaluate  
142 the potential role of Nrn1 expression in T cell tolerance development, we further examined Nrn1  
143 expression kinetics after T cell activation. Nrn1 expression was significantly induced after CD4<sup>+</sup>  
144 T cell activation (Figure 1D). Using a Nrn1 specific antibody, Nrn1 can be detected on activated  
145 CD4<sup>+</sup> and CD8<sup>+</sup> cells (Figure 1D, Figure 1-figure supplement 1C). The significant enhancement  
146 of Nrn1 expression after T cell activation suggests that Nrn1 may contribute to the process of T  
147 cell tolerance development and/or maintenance.

148 To understand the functional implication of Nrn1 expression in immune tolerance, we  
149 analyzed Nrn1-deficient (Nrn1<sup>-/-</sup>) mice (Fujino et al., 2011). In the first evaluation of the Nrn1<sup>-/-</sup>  
150 colony, Nrn1<sup>-/-</sup> mice had consistently reduced body weight compared to heterozygous Nrn1<sup>+/-</sup> and  
151 WT (Nrn1<sup>+/+</sup>) mice (Figure 1-figure supplement 2A). The lymphoid tissues of Nrn1<sup>-/-</sup> mice were  
152 comparable to their Nrn1<sup>+/-</sup> and WT counterparts except for a slight reduction in cell number that  
153 was observed in the spleens of Nrn1<sup>-/-</sup> mice, likely due to their smaller size (Figure 1-figure  
154 supplement 2B). Analysis of thymocytes revealed no defect in T cell development (Figure 1-figure  
155 supplement 2C), and a flow cytometric survey of the major immune cell populations in the  
156 peripheral lymphoid tissue of these mice revealed similar proportions of CD4, CD8 T cells, B cells,  
157 monocytes and dendritic cells (DCs) (Figure 1-figure supplement 2D). Similarly, no differences  
158 were found between the proportions of anergic and Treg cells in Nrn1<sup>-/-</sup>, Nrn1<sup>+/-</sup> and WT mice  
159 (Figure 1-figure supplement 2E, F), suggesting that Nrn1 deficiency does not significantly affect  
160 anergic and Treg cell balance under steady state. Additionally, histopathology assessment of lung,  
161 heart, liver, kidney, intestine and spleen harvested from 13 months old Nrn1<sup>-/-</sup> and Nrn1<sup>+/-</sup>  
162 littermates did not reveal any evidence of autoimmunity (data not shown). The comparable level  
163 of anergic and Treg cell population among Nrn1<sup>-/-</sup>, Nrn1<sup>+/-</sup> and WT mice and lack of autoimmunity

164 in *Nrn1*<sup>-/-</sup> aged mice suggest that *Nrn1* deficiency is not associated with baseline immune  
165 abnormalities or overt dysfunction. Due to the similarity between *Nrn1*<sup>+/-</sup> and WT mice, we have  
166 used either *Nrn1*<sup>+/-</sup> or WT mice as our control depending on mice availability and referred to both  
167 as “ctrl” in the subsequent discussion.

168 To evaluate the relevance of *Nrn1* in CD4<sup>+</sup> T cell tolerance development, we employed the  
169 classic peptide-induced T cell anergy model (Vanasek et al., 2006). Specifically, we crossed OVA  
170 antigen-specific TCR transgenic OTII mice onto the *Nrn1*<sup>-/-</sup> background. *Nrn1*<sup>-/-</sup>\_OTII<sup>+</sup> or  
171 control\_OTII<sup>+</sup> (ctrl\_OTII<sup>+</sup>) cells marked with Thy1.1<sup>+</sup> congenic marker (Thy1.1<sup>+</sup>Thy1.2<sup>-</sup>), were  
172 co-transferred with polyclonal WT Tregs (marked as Thy1.1<sup>-</sup>Thy1.2<sup>+</sup>), into TCR $\alpha$  knockout mice  
173 (TCR $\alpha$ <sup>-/-</sup>), followed by injection of soluble OVA peptide to induce clonal anergy (Figure 1E)  
174 (Chappert and Schwartz, 2010; Martinez et al., 2012; Mercadante and Lorenz, 2016; Shin et al.,  
175 2014). On day 13 after cell transfer, the proportion and number of OTII cells increased in the *Nrn1*<sup>-/-</sup>  
176 *Nrn1*<sup>-/-</sup>\_OTII compared to the ctrl\_OTII hosts (Figure 1F). Moreover, *Nrn1*<sup>-/-</sup>\_OTII cells produced  
177 increased IL2 than ctrl\_OTII upon restimulation (Figure 1G). Anergic CD4 Tconv cells can  
178 transdifferentiate into Foxp3<sup>+</sup> pTreg cells *in vivo* (DL, 2017; Kalekar et al., 2016; Kuczma et al.,  
179 2021). Consistent with reduced anergy induction, the proportion of Foxp3<sup>+</sup> pTreg among *Nrn1*<sup>-/-</sup>  
180 *Nrn1*<sup>-/-</sup>\_OTII was significantly reduced (Figure 1H). In parallel with the phenotypic analysis, we  
181 compared gene expression between *Nrn1*<sup>-/-</sup>\_OTII and ctrl\_OTII cells by RNA Sequencing  
182 (RNASeq). Gene set enrichment analysis (GSEA) revealed that the gene set on T cell anergy was  
183 enriched in ctrl relative to *Nrn1*<sup>-/-</sup>\_OTII cells (Figure 1I)(Safford et al., 2005). Also, consistent  
184 with the decreased transdifferentiation to Foxp3<sup>+</sup> cells, the Treg signature gene set was  
185 prominently reduced in *Nrn1*<sup>-/-</sup>\_OTII cells relative to the ctrl (Figure 1J). Anergic T cells are  
186 characterized by inhibition of proliferation and compromised effector cytokines such as IL2  
187 production (Choi and Schwartz, 2007). The increased cell expansion and cytokine production in  
188 *Nrn1*<sup>-/-</sup>\_OTII cells and the reduced expression of anergic and Treg signature genes all support the  
189 notion that *Nrn1* is involved in T cell anergy development.

190 Anergic T cells are developed after encountering antigen, passing through a brief effector  
191 stage, and reaching an anergic state (Chappert and Schwartz, 2010; Huang et al., 2003; Silva  
192 Morales and Mueller, 2018; Zha et al., 2006). Enhanced T cell activation, defective Treg cell  
193 conversion or expansion, and heightened T effector cell response may all contribute to defects in  
194 T cell anergy induction and/or maintenance (Chappert and Schwartz, 2010; Huang et al., 2003;

195 Kalekar et al., 2016; Silva Morales and Mueller, 2018; Zha et al., 2006). We first examined early  
196 T cell activation to understand the underlying cause of defective anergy development in *Nrn1*<sup>-/-</sup>  
197 cells. *Nrn1*<sup>-/-</sup> CD4<sup>+</sup> cells showed reduced T cell activation, as evidenced by reduced CellTrace  
198 violet dye (CTV) dilution, activation marker expression, and Ca<sup>++</sup> entry after TCR stimulation  
199 (Figure 1-figure supplement 3A, B, C). The reduced early T cell activation observed in *Nrn1*<sup>-/-</sup>  
200 CD4 cells suggests that the compromised anergy development in *Nrn1*<sup>-/-</sup> OTII cells was not caused  
201 by enhanced early T cell activation. The defective pTreg generation and/or enhanced effector T  
202 cell response may contribute to compromised anergy development.

### 203 **Compromised Treg expansion and suppression in the absence of *Nrn1*.**

204 The significant reduction of Foxp3<sup>+</sup> pTreg among *Nrn1*<sup>-/-</sup> OTII cells could be caused by  
205 the diminished conversion of Foxp3<sup>-</sup> Tconv cells to pTreg and/or diminished Treg cell expansion  
206 and persistence. To understand the cause of pTreg reduction in *Nrn1*<sup>-/-</sup> OTII cells (Figure 1H), we  
207 turned to the induced Treg (iTreg) differentiation system to evaluate the capability of Foxp3<sup>+</sup> Treg  
208 development and expansion in *Nrn1*<sup>-/-</sup> cells. Similar proportions of Foxp3<sup>+</sup> cells were observed in  
209 *Nrn1*<sup>-/-</sup> and ctrl cells under the iTreg culture condition, suggesting that *Nrn1* deficiency does not  
210 significantly impact Foxp3<sup>+</sup> cell differentiation. To examine the capacity of iTreg expansion, *Nrn1*<sup>-/-</sup>  
211 and ctrl iTreg cells were restimulated with anti-CD3, and we found reduced live cells over time  
212 in *Nrn1*<sup>-/-</sup> iTreg compared to the ctrl (Figure 2A). The reduced live cell number in *Nrn1*<sup>-/-</sup> was  
213 accompanied by reduced Ki67 expression (Figure 2B). Although *Nrn1*<sup>-/-</sup> iTregs retained a higher  
214 proportion of Foxp3<sup>+</sup> cells three days after restimulation, however, when taking into account the  
215 total number of live cells, the actual number of live Foxp3<sup>+</sup> cells was reduced in *Nrn1*<sup>-/-</sup> (Figure  
216 2C). Treg cells are not stable and are prone to losing Foxp3 expression after extended proliferation  
217 (Feng et al., 2014; Floess et al., 2007; Li et al., 2014; Zheng et al., 2010). The increased proportion  
218 of Foxp3<sup>+</sup> cells was consistent with reduced proliferation observed in *Nrn1*<sup>-/-</sup> cells. Thus, *Nrn1*  
219 deficiency can lead to reduced iTreg cell proliferation and persistence *in vitro*.

220 The defects observed in iTreg cell expansion *in vitro* prompt further examination of *Nrn1*<sup>-/-</sup>  
221 nTreg expansion and suppression function *in vivo*. To this end, we tested the suppression capacity  
222 of congenically marked (CD45.1<sup>+</sup>CD45.2<sup>+</sup>) *Nrn1*<sup>-/-</sup> or ctrl nTreg toward CD45.1<sup>+</sup>CD45.2<sup>-</sup>  
223 responder cells in Rag2<sup>-/-</sup> mice (Figure 2D). The CD45.1<sup>+</sup>CD45.2<sup>-</sup> responder cells devoid of Treg  
224 cells were splenocytes derived from Foxp3DTRGFP (FDG) mice pretreated with diphtheria toxin  
225 (DT) (Kim et al., 2007; Workman et al., 2011). DT treatment caused the deletion of Treg cells in



226 FDG mice (Kim et al., 2007). Although the CD45.1<sup>-</sup>CD45.2<sup>+</sup> Nrn1<sup>-/-</sup> and ctrl cell proportions were  
227 not significantly different among hosts splenocytes at day 7 post transfer (Figure 2E), Nrn1<sup>-/-</sup> cells  
228 retained a higher Foxp3<sup>+</sup> cell proportion and reduced Ki67 expression comparing to the ctrl (Figure  
229 2F, G). These findings were similar to our observation of iTreg cells *in vitro* (Figure 2B, C). Nrn1<sup>-</sup>  
230 <sup>-</sup> Tregs also showed reduced suppression toward CD45.1<sup>+</sup> responder cells, evidenced by increased  
231 CD45.1<sup>+</sup> proportion and cell number in host splenocytes (Figure 2H).

232 To evaluate the functional implication of Nrn1<sup>-/-</sup> Treg suppression in disease settings, we  
233 challenged the Rag2<sup>-/-</sup> hosts with the poorly immunogenic B16F10 tumor (Figure 2D). Tumors  
234 grew much slower in Nrn1<sup>-/-</sup> Treg recipients than those reconstituted with ctrl Tregs (Figure 2I).  
235 Moreover, the number of CD45.1<sup>+</sup> cells in tumor-draining lymph nodes and spleens increased  
236 significantly in Nrn1<sup>-/-</sup> Treg hosts compared to the ctrl group (Figure 2J). Consistently, the  
237 CD45.1<sup>+</sup> responder cell proportion among tumor lymphocyte infiltrates (TILs) was also increased  
238 (Figure 2K), accompanied by an increased proportion of IFN $\gamma$ <sup>+</sup> cells among CD8 TILs from Nrn1<sup>-</sup>  
239 <sup>-</sup> Treg hosts (Figure 2L). The increased expansion of CD45.1<sup>+</sup> responder cells and reduced tumor  
240 growth further confirmed the reduced suppressive capacity of Nrn1<sup>-/-</sup> Treg cells.

#### 241 **Nrn1 impacts Treg cell electrical and metabolic state**

242 To understand the molecular mechanisms associated with Nrn1<sup>-/-</sup> Treg cells, we compared  
243 gene expression between Nrn1<sup>-/-</sup> and ctrl iTregs under resting (IL2 only) and activation (aCD3 and  
244 IL2) conditions by RNASeq. GSEA on gene ontology database and clustering of enriched gene  
245 sets by Cytoscape identified three clusters enriched in resting Nrn1<sup>-/-</sup> iTreg (Figure 3A, Figure 3-  
246 figure supplement Table 1)(Shannon et al., 2003; Subramanian et al., 2005). The “neurotransmitter  
247 involved in membrane potential (MP)” and “sodium transport” clusters involved gene sets on the  
248 ion transport and cell MP regulation (Figure 3A, Figure 3-figure supplement Table 1). MP is the  
249 difference in electric charge between the interior and the exterior of the cell membrane (Abdul  
250 Kadir et al., 2018; Blackiston et al., 2009; Ma et al., 2017). Ion channels and transporters for Na<sup>+</sup>  
251 and other ions such as K<sup>+</sup>, Cl<sup>-</sup> *et al.* maintain the ion balance and contribute to cell MP (Blackiston  
252 et al., 2009). MP change can impact cell plasma membrane lipid dynamics and affect receptor  
253 kinase activity (Zhou et al., 2015). The enrichment of “receptor protein kinase” gene set clusters  
254 may reflect changes caused by MP (Figure 3A, Figure 3-figure supplement Table 1). Gene set  
255 cluster analysis on activated iTreg cells also revealed the enrichment of the “ion channel and  
256 receptor” cluster in Nrn1<sup>-/-</sup> cells (Figure 3B, Figure 3-figure supplement table 2), supporting the



257 potential role of *Nrn1* in modulating ion balances and MP.

258 The “Neurotransmitter receptor activity involved in regulation of postsynaptic membrane  
259 potential” gene set was significantly enriched under resting and activation conditions (Figure 3C  
260 and D; Figure 3-figure supplement Table 3). The  $\alpha$ -amino-3-hydroxy-5-methyl-4-  
261 isoxazolepropionic acid receptor (AMPA) subunits *Gria2* and *Gria3* are the major components  
262 of this gene set and showed increased expression in *Nrn1*<sup>-/-</sup> cells (Figure 3D). AMPAR is an  
263 ionotropic glutamate receptor that mediates fast excitatory synaptic transmission in neurons. *Nrn1*  
264 has been reported as an accessory protein for AMPAR (Pandya et al., 2018; Schwenk et al., 2012;  
265 Subramanian et al., 2019), although the functional implication of *Nrn1* as an AMPAR accessory  
266 protein remains unclear. The enrichment of MP related gene set prompted the examination of  
267 electric status, including MP level and ion channel expressions. We examined the relative MP level  
268 by FLIPR MP dye, a lipophilic dye able to cross the plasma membrane, which has been routinely  
269 used to measure cell MP changes (Dvorak et al., 2021; Joesch et al., 2008; Nik et al., 2017;  
270 Whiteaker et al., 2001). When the cells are depolarized, the dye enters the cells, causing an increase  
271 in fluorescence signal. Conversely, cellular hyperpolarization results in dye exit and decreased  
272 fluorescence. Compared to ctrl iTreg cells, *Nrn1*<sup>-/-</sup> exhibits significant hyperpolarization under  
273 both resting and activation conditions (Figure 3E). Consistent with the MP change, the “MF\_metal  
274 ion transmembrane transporter activity” gene set, which contains 436 ion channel related genes,  
275 was significantly enriched and showed a different expression pattern in *Nrn1*<sup>-/-</sup> iTregs (Figure 3F;  
276 Figure 3-figure supplement 1A and B). The changes in cellular MP and differential expression of  
277 ion channel and transporter genes in *Nrn1*<sup>-/-</sup> implicate the role of *Nrn1* in the balance of electric  
278 state in the iTreg cell.

279 MP changes have been associated with changes in amino acid (AA) transporter expression  
280 and nutrient acquisition, which in turn influences cellular metabolic and functional state (Yu et al.,  
281 2022). To understand whether MP changes in *Nrn1*<sup>-/-</sup> are associated with changes in nutrient  
282 acquisition and thus the metabolic state, we surveyed AA transport-related gene expression using  
283 the “Amino acid transmembrane transporter activity” gene set and found differential AA  
284 transporter gene expression between *Nrn1*<sup>-/-</sup> and ctrl iTregs (Figure 3G). Electrolytes and AAs  
285 entry are critical regulators of mTORC1 activation and T cell metabolism (Liu and Sabatini, 2020;  
286 Saravia et al., 2020; Sinclair et al., 2013; Wang et al., 2020). We examined mTORC1 activation  
287 at the protein level by evaluating mTOR and S6 phosphorylation via flow cytometry. We found

288 reduced phosphorylation of mTOR and S6 in activated *Nrn1*<sup>-/-</sup> iTreg cells (Figure 3H). We further  
289 performed a nutrient-sensing assay to evaluate the role of ion and nutrient entry in mTORC1  
290 activation. *Nrn1*<sup>-/-</sup> and ctrl iTreg cells were starved for one hour in a nutrient-free buffer, followed  
291 by adding RPMI medium with complete ions and nutrients, and cultured for two more hours. While  
292 adding the medium with nutrients clearly increased the mTOR and S6 phosphorylation, the degree  
293 of change was significantly less in *Nrn1*<sup>-/-</sup> than in the ctrl (Figure 3I). Consistently, GSEA on  
294 Hallmark gene sets reveal reduced gene set enrichment relating to the mTORC1 signaling,  
295 corroborating the reduced pmTOR and pS6 detection in *Nrn1*<sup>-/-</sup> cells. Moreover, *Nrn1*<sup>-/-</sup> cells also  
296 showed reduced expression of glycolysis, fatty acid metabolism, and oxidative phosphorylation  
297 related gene sets under both resting and activating conditions (Figure 3J, Figure 3-figure  
298 supplement 1C), indicating changes in metabolic status. Since previous work has identified  
299 mTORC1 to be an important regulator of aerobic glycolysis and given that our GSEA data  
300 suggested changes in glycolysis (Figure 3J) (Salmond, 2018), we performed the Seahorse assay  
301 and confirmed reduced glycolysis among *Nrn1*<sup>-/-</sup> cells (Figure 3K). Examination of mitochondrial  
302 bioenergetic function revealed a similar oxygen consumption rate (OCR) between *Nrn1*<sup>-/-</sup> and ctrl  
303 cells (Figure 3K). Thus, *Nrn1* expression can affect the iTreg electric state, influence ion channel  
304 and nutrient transporter expression, impact nutrient sensing, modulate metabolic state, and  
305 contribute to Treg expansion and suppression function.

### 306 ***Nrn1* impact effector T cell inflammatory response.**

307 CD4<sup>+</sup> T cells can pass through an effector stage on their way to an anergic state (Huang et  
308 al., 2003). Since *Nrn1* expression is significantly induced after T cell activation (Figure 1D), *Nrn1*  
309 might influence CD4<sup>+</sup> effector (T<sub>e</sub>) cell differentiation, affecting anergy development. *Nrn1* may  
310 exert different electric changes due to distinct ion channel expression contexts in T<sub>e</sub> cells than in  
311 Tregs. We first evaluated *Nrn1*<sup>-/-</sup> T<sub>e</sub> cell differentiation *in vitro*. *Nrn1* deficient CD4 T<sub>e</sub> cells  
312 showed increased Ki67 expression, associated with increased cytokine TNF $\alpha$ , IL2, and IFN $\gamma$   
313 expression upon restimulation (Figure 4A). To evaluate *Nrn1*<sup>-/-</sup> T<sub>e</sub> cell response *in vivo*, we crossed  
314 *Nrn1*<sup>-/-</sup> with FDG mice and generated *Nrn1*<sup>-/-</sup>\_FDG and ctrl\_FDG mice, which enabled the  
315 elimination of endogenous Treg cells (Figure 4B). Deleting endogenous Foxp3<sup>+</sup> Treg cells using  
316 DT will cause the activation of self-reactive T cells, leading to an autoimmune response (Kim et  
317 al., 2007; Nystrom et al., 2014). Upon administration of DT, we observed accelerated weight loss  
318 in *Nrn1*<sup>-/-</sup>\_FDG mice, reflecting enhanced autoimmune inflammation (Figure 4C). Examination of

319 T cell response revealed a significant increase in Ki67 expression and inflammatory cytokine  
320  $\text{TNF}\alpha$ , IL2, and  $\text{IFN}\gamma$  expression among  $\text{Nrnl}^{-/-}$  CD4 cells on day 6 post DT treatment (Figure 4D),  
321 consistent with the findings *in vitro*. The proportion of  $\text{Foxp3}^+$  cells was very low on day 6 post  
322 DT treatment and comparable between  $\text{Nrnl}^{-/-}$  and the ctrl (Figure 4E), suggesting that the  
323 differential Te cell response was not due to the impact from Treg cells. Thus,  $\text{Nrnl}$  deficiency  
324 enhances Te cell response *in vitro* and *in vivo*.

325 To identify molecular changes responsible for  $\text{Nrnl}^{-/-}$  Te phenotype, we compared gene  
326 expression between  $\text{Nrnl}^{-/-}$  and ctrl Te cells by RNASeq. GSEA and Cytoscape analysis identified  
327 a cluster of gene sets on “membrane repolarization”, suggesting that  $\text{Nrnl}$  may also be involved  
328 in the regulation of MP under Te context (Figure 4F, Figure 4-figure supplement Table 4)  
329 (Shannon et al., 2003; Subramanian et al., 2005). While the “membrane\_repolarization” gene set  
330 was enriched in  $\text{Nrnl}^{-/-}$  (Figure 4G), the “Neurotransmitter receptor activity involved in regulation  
331 of postsynaptic membrane potential” gene set was no longer enriched, but the AMPAR subunit  
332  $\text{Gria3}$  expression was still elevated in  $\text{Nrnl}^{-/-}$  Te cells (Figure 4-figure supplement 1A). Although  
333 MP in Te cells was comparable between  $\text{Nrnl}^{-/-}$  and ctrl (Figure 4H), the “MF\_metal ion  
334 transmembrane transporter activity” gene set was significantly enriched in  $\text{Nrnl}^{-/-}$  with different  
335 gene expression patterns (Figure 4I, Figure 4-figure supplement 1B), indicative of different electric  
336 state. The significant enrichment of ion channel related genes in  $\text{Nrnl}^{-/-}$  Te cells was in line with  
337 the finding in  $\text{Nrnl}^{-/-}$  iTreg cells, supporting the notion that  $\text{Nrnl}$  expression may be involved in  
338 ion balance and MP modulation.

339 Examination of nutrient transporters revealed that the “Amino acid transmembrane  
340 transporter activity” gene set was significantly enriched in  $\text{Nrnl}^{-/-}$  cells than the ctrl (Figure 4J).  
341 Along with the enrichment of ion channel and nutrient transporter genes (Figure 4I and J), we  
342 found enhanced mTOR and S6 phosphorylation in  $\text{Nrnl}^{-/-}$  Te cells (Figure 4K). We also compared  
343 nutrient sensing capability between  $\text{Nrnl}^{-/-}$  and ctrl Te cells, as outlined in Figure 3I.  $\text{Nrnl}^{-/-}$  Te  
344 showed increased mTOR and S6 phosphorylation after sensing ions and nutrients in RPMI medium  
345 (Figure 4L), confirming the differential impact of ions and nutrients on  $\text{Nrnl}^{-/-}$  and ctrl Te cells.  
346 GSEA on Hallmark collection showed enrichment of mTORC1 signaling gene set (Figure 4M),  
347 corroborating with increased pmTOR and pS6 detection in  $\text{Nrnl}^{-/-}$  Te cells. Along with increased  
348 mTORC1 signaling,  $\text{Nrnl}^{-/-}$  Te cells also showed enrichment of gene sets on glycolysis and  
349 proliferation (Figure 4M). Evaluation of metabolic changes by seahorse confirmed increased

350 glycolysis in *Nrn1*<sup>-/-</sup> cells, while the OCR remained comparable between *Nrn1*<sup>-/-</sup> and ctrl (Figure  
351 4N). These *in vitro* studies on Te cells indicate that *Nrn1* deficiency resulted in the dysregulation  
352 of the electrolyte and nutrient transport program, impacting Te cell nutrient sensing, metabolic  
353 state, and the outcome of inflammatory response.

### 354 ***Nrn1* deficiency exacerbates autoimmune disease**

355 The coordinated reaction of Treg and Te cells contributes to the outcome of the immune  
356 response. We employed the experimental autoimmune encephalomyelitis (EAE), the murine  
357 model of multiple sclerosis (MS) to evaluate the overall impact of *Nrn1* on autoimmune disease  
358 development. Upon EAE induction, the incidence and time to EAE onset in *Nrn1*<sup>-/-</sup> mice were  
359 comparable to the ctrl mice, but the severity, disease persistence, and body weight loss were  
360 increased in *Nrn1*<sup>-/-</sup> mice (Figure 5A). Exacerbated EAE was associated with significantly  
361 increased CD45<sup>+</sup> cell infiltrates, increased CD4<sup>+</sup> cell number, increased proportion of MOG-  
362 specific CD4 cells, and reduced proportion of Foxp3<sup>+</sup> CD4 cells in the *Nrn1*<sup>-/-</sup> spinal cord (Figure  
363 5B-E). Moreover, we also observed increased proportions of IFN $\gamma$ <sup>+</sup> and IL17<sup>+</sup> CD4 cells in *Nrn1*<sup>-/-</sup>  
364 mice (Figure 5F). Thus, the results from EAE corroborated with earlier data and confirmed the  
365 important role of *Nrn1* in establishing immune tolerance and modulating autoimmunity.

366

### 367 **Discussion**

368 T cell expansion and functional development depend on adaptive electric and metabolic  
369 changes, maintaining electrolyte balances, and appropriate nutrient uptake. The negative charge of  
370 the plasma membrane, ion channel expression pattern, and function are key characteristics  
371 associated with the cellular electric state in different systems, impacting cell proliferation and  
372 function (Blackiston et al., 2009; Emmons-Bell and Hariharan, 2021; Kiefer et al., 1980; Monroe  
373 and Cambier, 1983; Sundelacruz et al., 2009). The electrolytes and nutrients, including amino  
374 acids, metabolites, and small peptides transported through ion channels and nutrient transporters,  
375 are also regulators and signaling agents impacting the choice of cellular metabolic pathways and  
376 functional outcomes (Hamill et al., 2020). In this study, we report that the neurotropic factor *Nrn1*  
377 expression influences CD4 T cell MP, ion channels, and nutrient transporter expression patterns,  
378 contributing to differential metabolic states in Treg and Te cells. *Nrn1* deficiency compromises  
379 Treg cell expansion and suppression while enhancing Te cell inflammatory response, exacerbating  
380 autoimmune disease.

381 Bioelectric controls have been defined as a type of epigenetics that can control information  
382 residing outside of genomic sequence (Levin, 2021). The sum of ion channels and pump activity  
383 generates the ionic gradient across the cell membrane, establishing the MP level and bioelectric  
384 state. Cells with the same MP can have different ion compositions, and the same ion channel may  
385 have a differential impact on MP when in combination with different ion channels (Abdul Kadir  
386 et al., 2018). Consistent with this notion, *Nrn1* deficiency has differential impacts on the cellular  
387 electric state under the Treg and Te cells with different ion channel combinations. Altered MP was  
388 detected in *Nrn1* deficient Treg cells (Figure 3E), while comparable MP was observed between  
389 *Nrn1*<sup>-/-</sup> and ctrl Te cells (Figure 4H). The MP level determined by ion channels and pump activity  
390 can influence the nutrient transport pattern, establishing a metabolic and functional state matching  
391 the MP level (Blackiston et al., 2009; Emmons-Bell and Hariharan, 2021; Kiefer et al., 1980;  
392 Monroe and Cambier, 1983; Sundelacruz et al., 2009; Yu et al., 2022). Yu et al. reported that  
393 macrophage MP modulates plasma membrane phospholipid dynamics and facilitates cell surface  
394 retention of nutrient transporters, thus supporting nutrient uptake and impacting the inflammatory  
395 response (Yu et al., 2022). Nutrient transport is key to T cell fate decisions and has been considered  
396 signal 4 to T cell fate choices (Chapman and Chi, 2022; Long et al., 2021). The changes in ion  
397 channel related gene expression and MP level in *Nrn1*<sup>-/-</sup> cells were accompanied by differential  
398 expression of AA transporter genes and nutrient sensing activity that impacted mTORC1 pathway  
399 activation and cellular glycolytic state (Figures 3 and 4). These results corroborate previous  
400 observations on the connection of MP in nutrient acquisition and metabolic change and support  
401 the role of *Nrn1* in coordinating T cell electric and metabolic adaptation (Yu et al., 2022).

402 Although *Nrn1*, as a small GPI-anchored protein, does not have channel activity by itself,  
403 it has been identified as one of the components in the AMPAR complex (Pandya et al., 2018;  
404 Schwenk et al., 2012; Subramanian et al., 2019). Na<sup>+</sup>-influx through the AMPA type ionotropic  
405 glutamate receptor can quickly depolarize the postsynaptic compartment and potentiate synaptic  
406 transmission in neurons. We have observed increased expression of AMPAR subunits in *Nrn1*<sup>-/-</sup>  
407 iTreg and Te cells (Figure 3D, Figure 4-figure supplement 1), implicating potential change in  
408 AMPAR activity in *Nrn1*<sup>-/-</sup> under Treg and Te cell context. Glutamate secreted by proliferating  
409 cells may influence T cell function through AMPAR. High glutamate levels are detected at the  
410 autoimmune disease site and tumor interstitial fluid (Bonnet et al., 2020; McNearney et al., 2004;  
411 Sullivan et al., 2019). Moreover, AMPAR has been implicated in exacerbating autoimmune

412 disease (Bonnet et al., 2015; Sarchielli et al., 2007). The increased expression of AMPAR subunits  
413 in *Nrn1*<sup>-/-</sup> cells supports the potential connection of *Nrn1* and AMPAR and warrants future  
414 investigation on the possibility that *Nrn1* functions through AMPAR, impacting T cell electric  
415 change. Besides AMPAR, *Nrn1* has been reported to function through the insulin receptor and  
416 fibroblast growth factor pathway (Shimada et al., 2016; Yao et al., 2012). Subramanian et al have  
417 suggested that rather than a traditional ligand with its cognate receptor, *Nrn1* may function as an  
418 adaptor to receptors to perform diverse cell-type-specific functions (Subramanian et al., 2019).  
419 Our results do not rule out these possibilities.

420 Overall, we found that *Nrn1* expression in Treg and Te cells can impact cellular electric  
421 state, nutrient sensing, and metabolism in a cell context dependent manner. The predominant  
422 enrichment of ion channel related gene sets in both Treg and Te cell context underscores the  
423 importance of *Nrn1* in modulating ion balance and MP. The changes in ion channels and nutrient  
424 transporter expression in Treg and Te cells and associated functional consequences highlight the  
425 importance of *Nrn1* in coordinating cell metabolic changes through channels and transporters  
426 during the adaptive response and contribute to the balance of tolerance and immunity.

427

## 428 **Materials and Methods**

### 429 **Mouse models.**

430 The *Nrn1*<sup>-/-</sup> mice (Fujino et al., 2011), Foxp3DTRGFP (FDG)(Kim et al., 2007), and TCR $\alpha$ <sup>-/-</sup> mice  
431 were obtained from the Jackson Laboratory. OTII mice on Thy1.1<sup>+</sup> background was kindly  
432 provided by Dr. Jonathan Powell. Rag2<sup>-/-</sup> mice were maintained in our mouse facility. 6.5 TCR  
433 transgenic mice specific for HA antigen and C3HA mice (both on the B10.D2 background) have  
434 been described previously (Huang et al., 2004). *Nrn1*<sup>-/-</sup> mice were crossed with OTII mice to  
435 generate *Nrn1*<sup>-/-</sup>\_OTII<sup>+</sup> mice, ctrl\_OTII<sup>+</sup> mice. *Nrn1*<sup>-/-</sup> mice were also crossed with FDG mice to  
436 generate *Nrn1*<sup>-/-</sup>\_FDG and ctrl\_FDG mice. All mice colonies were maintained in accordance with  
437 the guidelines of Johns Hopkins University and the institutional animal care and use committee

438

### 439 **Antibodies and Reagents.**

440 We have used the following antibodies: Anti-CD3 (17A2), anti-CD4 (RM4-5), anti-CD8a (53-6.7),  
441 anti-CD25 (PC61), anti-CD45.1 (A20), anti-CD45.2 (104), anti-CD62L (MEL-14), CD73  
442 (TY/111.8), anti-CD90.1 (OX-7), anti-CD90.2 (30-H12), anti-TCR V $\alpha$ 5.1, 5.2 (MR9-4), anti-



443 PD1 (29F.1A12), anti-IFN $\gamma$  (XMG1.2), anti-IL17 $\alpha$  (TC11-18H10.1), anti-TNF $\alpha$  (MP6-XT22),  
444 anti-Tbet (4B10), anti-Ki67 (16A8) were purchased from Biolegend. Anti-CD44 (IM7), CD45  
445 (30-F11), anti-CD69(H1.2F3) were purchased from BD Bioscience. Anti-FOXP3 (FJK-16s) was  
446 purchased from eBioscience. The flow cytometry data were collected using BD Celesta (BD  
447 Biosciences) or Attune Flow Cytometers (ThermoFisher). Data were analyzed using FlowJo (Tree  
448 Star) software.

449 Mouse monoclonal anti-Nrn1 antibody (Ab) against Nrn1 was custom-made (A&G  
450 Pharmaceutical). The specificity of anti-Nrn1 Ab was confirmed by ELISA, cell surface staining  
451 of Nrn1 transfected 293T cells, and western blot of Nrn1 recombinant protein and brain protein  
452 lysate from WT mice or Nrn1<sup>-/-</sup> mice (data not shown). OVA<sub>323-339</sub> peptide and MOG<sub>35-55</sub> was  
453 purchased from GeneScript. Incomplete Freund's adjuvant (IFA) and Mycobacterium tuberculosis  
454 H37Ra (killed and desiccated) were purchased from Difco. Pertussis toxin was purchased from  
455 List Biological Laboratories and diphtheria toxin was obtained from Millipore-Sigma.

456

#### 457 **Cell purification and culture.**

458 Naïve CD4 cells were isolated from the spleen and peripheral lymph node by a magnetic bead-  
459 based purification according to the manufacturer's instruction (Miltenyi Biotech). Purified CD4  
460 cells were stimulated with plate-bound anti-CD3 (5ug/ml, Bio-X-Cell) and anti-CD28 (2ug/ml,  
461 Bio-X-Cell) for 3 days, in RPMI1640 medium supplemented with 10%FBS, HEPES,  
462 penicillin/streptomycin, MEM Non-Essential Amino Acids, and  $\beta$ -mercaptoethanol. For iTreg cell  
463 differentiation, cells were stimulated in the presence of human IL2 (100u/ml, PeproTech), human  
464 TGF $\beta$  (10ng/ml, PeproTech), anti-IL4, and anti-IFN $\gamma$  antibody (5ug/ml, Clone 11B11 and clone  
465 XMG1.2, Bio-X-Cell) in 10% RPMI medium. CD4<sup>+</sup> Te cells were differentiated without  
466 additional cytokine or antibody for three days, followed by additional culture for 2 days in IL2  
467 100u/ml in 10%RPMI medium. nTreg cells were isolated by sorting from the FDG CD4<sup>+</sup> fraction  
468 based on Foxp3<sup>+</sup>GFP and CD25 expression (CD4<sup>+</sup>CD25<sup>+</sup>GFP<sup>+</sup>). Alternatively, nTreg cells were  
469 enriched from CD4 cells by positive selection using the CD4<sup>+</sup>CD25<sup>+</sup> Regulatory T Cell Isolation  
470 Kit from Miltenyi.

471

#### 472 **Self-antigen induced tolerance model.**

473 1x10<sup>6</sup> HA-specific Thy1.1<sup>+</sup> 6.5 CD4 cells from donor mice on a B10.D2 background were



474 transferred into C3-HA recipient mice, where HA is expressed as self-antigen in the lung; or into  
475 WT B10.D2 mice followed by infection with Vac-HA virus ( $1 \times 10^6$  pfu). HA-reactive T cells were  
476 recovered from the lung-draining lymph node of C3-HA host mice or WT B10.D2 Vac-HA  
477 infected mice at indicated time points by cell sorting. RNA from sorted cells was used for qRT-  
478 PCR assay examining *Nrn1* expression.

479

#### 480 **Peptide-induced T cell anergy model.**

481  $5 \times 10^5$  Polyclonal Treg cells from CD45.1<sup>+</sup> C57BL/6 mice were mixed with  $5 \times 10^6$  thy1.1<sup>+</sup> OTII  
482 cells from *Nrn1*<sup>-/-</sup> OTII or ctrl\_OTII mice and transferred by *i.v.* injection into TCR $\alpha$ <sup>-/-</sup> mice.  
483 100ug of OVA<sub>323-339</sub> dissolved in PBS was administered *i.v.* on days 1, 4, and 7 after cell transfer.  
484 Host mice were harvested on day 13 after cell transfer, and cells from the lymph node and spleen  
485 were further analyzed.

486

#### 487 ***In vivo* Treg suppression assay.**

488 nTreg cells from CD45.2<sup>+</sup>CD45.1<sup>-</sup> *Nrn1*<sup>-/-</sup> or ctrl mice ( $5 \times 10^5$ /mouse) in conjunction with CD45.1<sup>+</sup>  
489 splenocytes ( $2 \times 10^6$ /mouse) from FDG mice were cotransferred *i.p.* into Rag2<sup>-/-</sup> mice. The CD45.1<sup>+</sup>  
490 splenocytes were obtained from FDG mice pretreated with DT for 2 days to deplete Treg cells.  
491 Treg suppression toward CD45.1<sup>+</sup> responder cells was assessed on day 7 post cell transfer.  
492 Alternatively, 7 days after cell transfer, Rag2<sup>-/-</sup> hosts were challenged with an *i.d.* inoculation of  
493 B16F10 cells ( $1 \times 10^5$ ). Tumor growth was monitored daily. Treg-mediated suppression toward  
494 anti-tumor response was assessed by harvesting mice day 18-21 post-tumor inoculation.

495

#### 496 **Induction of autoimmunity by transient Treg depletion.**

497 To induce autoimmunity in *Nrn1*<sup>-/-</sup>\_FDG and ctrl\_FDG mice, 1ug/mouse of DT was administered  
498 *i.p.* for two consecutive days, and the weight loss of treated mice was observed over time.

499

#### 500 **EAE induction**

501 EAE was induced in mice by subcutaneous injection of 200  $\mu$ g MOG<sub>35-55</sub> peptide with 500  $\mu$ g M.  
502 tuberculosis strain H37Ra (Difco) emulsified in incomplete Freund Adjuvant oil in 200ul volume  
503 into the flanks at two different sites. In addition, the mice received 400 ng pertussis toxin (PTX;  
504 List Biological Laboratories) *i.p.* at the time of immunization and 48 h later. Clinical signs of EAE

505 were assessed daily according to the standard 5-point scale (Miller et al., 2007): normal mouse; 0,  
506 no overt signs of disease; 1, limp tail; 2, limp tail plus hindlimb weakness; 3, total hindlimb  
507 paralysis; 4, hindlimb paralysis plus 75% of body paralysis (forelimb paralysis/weakness); 5,  
508 moribund.

509

## 510 **ELISA**

511 MaxiSorp ELISA plates (ThermoScientific Nunc) were coated with 100  $\mu$ l of 1 $\mu$ g/ml anti-mIL-2  
512 (BD Pharmingen #554424) at 4°C overnight. Coated plates were blocked with 200 $\mu$ l of blocking  
513 solution (10%FBS in PBS) for 1hr at room temperature (RT) followed by incubation of culture  
514 supernatant and mIL-2 at different concentrations as standard. After 1hr, plates were washed and  
515 incubated with anti-mIL-2-biotin (BD Pharmingen #554426) at RT for 1hr. After 1hr, plates were  
516 incubated with 100 $\mu$ l of horseradish peroxidase-labeled avidin (Vector Laboratory, #A-2004)  
517 1 $\mu$ g/ml for 30min. After washing, samples were developed using the KPL TMB Peroxidase  
518 substrate system (Seracare #5120-0047) and read at 405 or 450 nm after the addition of the stop  
519 solution.

520

## 521 **Quantitative RT-PCR**

522 RNA was isolated using the RNeasy Micro Kit (Qiagen 70004) following the manufacturer's  
523 instructions. RNA was converted to cDNA using the High-Capacity cDNA Reverse Transcription  
524 Kit (ThermoFisher Scientific #4368814) according to the manufacturer's instructions. The primers  
525 of murine genes were purchased from Integrated DNA Technology (IDT). qPCR was performed  
526 using the PowerUp SYBR Green Master Mix (ThermoFisher Scientific #A25780) and the Applied  
527 Biosystems StepOnePlus 96-well real-time PCR system. Gene expression levels were calculated  
528 based on the Delta-Delta Ct relative quantification method. Primers used for Nrn1 PCR were as  
529 follows: GCGGTGCAAATAGCTTACCTG (forward); CGGTCTTGATGTTTCGTCTTGTC  
530 (reverse).

531

## 532 **Ca<sup>++</sup> flux and Membrane potential measurement**

533 To measure Ca<sup>++</sup> flux, CD4 cells were loaded with Fluo4 dye at 2 $\mu$ M in the complete cell culture  
534 medium at 37°C for 30min. Cells were washed and resuspended in HBSS Ca<sup>++</sup> free medium and  
535 plated into 384 well glass bottom assay plate (minimum of 4 wells per sample). Ca<sup>++</sup> flux was

536 measured using the FDSS6000 system (Hamamatsu Photonics). To measure store-operated  
537 calcium entry (SOCE), after the recording of the baseline T cells  $\text{Ca}^{++}$  fluorescent for 1min,  
538 thapsigargin (TG) was added to induce store  $\text{Ca}^{++}$  depletion, followed by the addition of  $\text{Ca}^{++}$   $2\mu\text{M}$   
539 in the extracellular medium to observe  $\text{Ca}^{++}$  cellular entry.

540 Membrane potential was measured using FLIPR Membrane Potential Assay kit (Molecular devices)  
541 according to the manufacturer's instructions. Specifically, T cells were loaded with FLIPR dye by  
542 adding an equal volume of FLIPR dye to the cells and incubated at  $37^{\circ}\text{C}$  for 30 minutes. Relative  
543 membrane potential was measured by detecting FLIPR dye incorporation using flow cytometry.

544

#### 545 **Extracellular flux analysis (Seahorse assays).**

546 Real-time measurements of extracellular acidification rate (ECAR) and oxygen consumption rate  
547 (OCR) were performed using an XFe-96 Bioanalyser (Agilent). T cells ( $2 \times 10^5$  cells per well;  
548 minimum of four wells per sample) were spun into previously poly-d-lysine-coated 96-well plates  
549 (Seahorse) in complete RPMI-1640 medium. ECAR was measured in RPMI medium in basal  
550 condition and in response to 25mM glucose,  $1\mu\text{M}$  oligomycin, and 50mM of 2-DG (all from Sigma  
551 Aldrich). OCR was measured in RPMI medium supplemented with 25mM glucose, 2mM L-  
552 glutamine, and 1mM sodium pyruvate, under basal condition and in response to  $1\mu\text{M}$  oligomycin,  
553  $1.5\mu\text{M}$  of carbonylcyanide-4-(trifluoromethoxy)-phenylhydrazone (FCCP) and  $1\mu\text{M}$  of rotenone  
554 and antimycin (all from Sigma Aldrich).

555

#### 556 **RNAseq and data analysis**

557 RNASeq samples: 1. Anergic T cell analysis. Ctrl and  $\text{Nrnl}^{-/-}$  OTII cells were sorted from the host  
558 mice (n=3 per group). 2. iTreg cell analysis. In vitro differentiated  $\text{Nrnl}^{-/-}$  and ctrl iTreg cells were  
559 replated in resting condition (IL2 100u/ml) or stimulation condition (IL2 100u/ml and aCD3  
560 5ug/ml). Cells were harvested 20 hr after replating for RNASeq analysis. 3. Effector T cells.  $\text{Nrnl}^{-/-}$   
561 and ctrl CD4 Tn cells were activated for 3 days (aCD3 5ug/ml, aCD28 2ug/ml), followed by  
562 replating in IL2 medium (100u/ml). Te cells were harvested two days after replating and subjected  
563 to RNASeq analysis.

564 RNA-sequencing analysis was performed by Admera Health (South Plainfield, NJ). Read quality  
565 was assessed with FastQC and aligned to the Mus Musculus genome (Ensembl GRCm38) using  
566 STAR aligner (version 2.6.0)(Dobin et al., 2013). Aligned reads were counted using HTSeq

567 (version 0.9.0)(Anders et al., 2015), and the counts were loaded into R (The R Foundation).  
568 DESeq2 package (version 1.24.0)(Love et al., 2014) was used to normalize the raw counts. GSEA  
569 was performed using public gene sets (HALLMARK, and GO)(Subramanian et al., 2005).  
570 Cytoscape was used to display enriched gene sets cluster (Shannon et al., 2003).  
571 Statistical analysis. All numerical data were processed using Graph Pad Prism 10. Data are  
572 expressed as the mean +/- the SEM, or as stated. Statistical comparisons were made using an  
573 unpaired student t-test or ANOVA with multiple comparison tests where 0.05 was considered  
574 significant, and a normal distribution was assumed. The p values are represented as follows: \*  
575  $p < 0.05$ ; \*\*  $p < 0.01$ ; \*\*\*  $p < 0.001$ , \*\*\*\*  $p < 0.0001$ .

576

### 577 **Acknowledgements:**

578 This research is supported by grants from the Bloomberg-Kimmel Institute of JHU, the Melanoma  
579 Research Alliance, the National Institutes of Health (RO1AI099300 and RO1AI089830), and the  
580 Department of Defense (PC130767). JB's research was supported by a Crohn's and Colitis  
581 Foundation of America Research Fellowship, the Melanoma Research Foundation, and NCI grant  
582 P30CA016056.

583 We thank Dennis Gong for data processing and critical reading of the manuscript. We thank Dr.  
584 Elly Nedivi for providing polyclonal Nrn1 antibody and Dr. Fan Pan for reagent support. We thank  
585 Drs. Franck Housseau, Chien-Fu Hung for the constructive discussion of the project and the  
586 manuscript. We thank Drs. Hao Shi and Hongbo Chi for critical manuscript reading and helpful  
587 suggestions. We thank Dr. Rachel Helm for manuscript editing. We thank Drs. Richard L. Haganir,  
588 Bian Liu and Hana Goldschmidt for constructive discussion on Nrn1 and AMPAR connection.

### 589 **Author contributions:**

590 H. Y. was involved in all aspects of this study, including planning and performing experiments,  
591 analyzing and interpreting data, and writing the manuscript. H. N. and J. B. were involved in  
592 performing experiments and data interpretation. P. V., Y. Z., and A. L. analyzed Nrn1 expression  
593 in Treg cells and carried out Treg suppression and functional assay. M. M. was involved in Nrn1  
594 expression, Treg suppression assay, and manuscript writing. C. H. and C.D. conducted the anergy  
595 and Te cell differential gene expression study; Y.Z., J. F., and K. C. conducted an autoimmune  
596 inflammation study, and M. H. helped with mouse colony genotyping. X. Z. and Z. L. contributed  
597 to bioinformatic analysis. D.M. P. oversaw the project and was involved in data interpretation and

598 manuscript preparation.

599 **Competing interests:**

600 C.D. is a co-inventor on patents licensed from JHU to BMS and Janssen and is currently an  
601 employee of Janssen Research. D.M.P. is a consultant for Compugen, Shattuck Labs, WindMIL,  
602 Tempest, Immunai, Bristol-Myers Squibb, Amgen, Janssen, Astellas, Rockspring Capital,  
603 Immunomic, and Dracen; owns founders' equity in ManaT Bio Inc., WindMIL, Trex, Jounce,  
604 Enara, Tizona, Tieza, and RAPT; and receives research funding from Compugen, Bristol-Myers  
605 Squibb, and Enara. All other authors do not have conflicting financial interests.

606

607 **Data availability:**

608 The raw RNA sequencing data has been deposited under the GEO accession no. GSE121908 and  
609 GSE224083.

610

611

612

613

614

615

616

617

618

619

620

621

622

623

624

625

626

627

628

629 **References:**

- 630 Abdul Kadir, L., M. Stacey, and R. Barrett-Jolley. 2018. Emerging Roles of the Membrane  
631 Potential: Action Beyond the Action Potential. *Front Physiol* 9:1661.
- 632 Adler, A.J., D.W. Marsh, G.S. Yochum, J.L. Guzzo, A. Nigam, W.G. Nelson, and D.M. Pardoll.  
633 1998. CD4+ T cell tolerance to parenchymal self-antigens requires presentation by bone  
634 marrow-derived antigen-presenting cells. *The Journal of experimental medicine*  
635 187:1555-1564.
- 636 Anders, S., P.T. Pyl, and W. Huber. 2015. HTSeq--a Python framework to work with high-  
637 throughput sequencing data. *Bioinformatics* 31:166-169.
- 638 Babst, M. 2020. Regulation of nutrient transporters by metabolic and environmental stresses.  
639 *Curr Opin Cell Biol* 65:35-41.
- 640 Blackiston, D.J., K.A. McLaughlin, and M. Levin. 2009. Bioelectric controls of cell proliferation:  
641 ion channels, membrane voltage and the cell cycle. *Cell Cycle* 8:3527-3536.
- 642 Bohmwald, K., N.M.S. Gálvez, C.A. Andrade, V.P. Mora, J.T. Muñoz, P.A. González, C.A. Riedel,  
643 and A.M. Kalergis. 2021. Modulation of Adaptive Immunity and Viral Infections by Ion  
644 Channels. *Front Physiol* 12:736681.
- 645 Bonnet, C.S., S.J. Gilbert, E.J. Blain, A.S. Williams, and D.J. Mason. 2020. AMPA/kainate  
646 glutamate receptor antagonists prevent posttraumatic osteoarthritis. *JCI insight* 5:  
647 Bonnet, C.S., A.S. Williams, S.J. Gilbert, A.K. Harvey, B.A. Evans, and D.J. Mason. 2015.  
648 AMPA/kainate glutamate receptors contribute to inflammation, degeneration and pain  
649 related behaviour in inflammatory stages of arthritis. *Annals of the rheumatic diseases*  
650 74:242-251.
- 651 Buck, M.D., R.T. Sowell, S.M. Kaech, and E.L. Pearce. 2017. Metabolic Instruction of Immunity.  
652 *Cell* 169:570-586.
- 653 Cantalops, I., K. Haas, and H.T. Cline. 2000. Postsynaptic CPG15 promotes synaptic maturation  
654 and presynaptic axon arbor elaboration in vivo. *Nature neuroscience* 3:1004-1011.
- 655 Chapman, N.M., and H. Chi. 2022. Metabolic adaptation of lymphocytes in immunity and  
656 disease. *Immunity* 55:14-30.
- 657 Chappert, P., and R.H. Schwartz. 2010. Induction of T cell anergy: integration of environmental  
658 cues and infectious tolerance. *Current opinion in immunology* 22:552-559.
- 659 Chen, T.C., S.P. Cobbold, P.J. Fairchild, and H. Waldmann. 2004. Generation of anergic and  
660 regulatory T cells following prolonged exposure to a harmless antigen. *Journal of*  
661 *immunology (Baltimore, Md. : 1950)* 172:5900-5907.
- 662 Choi, S., and R.H. Schwartz. 2007. Molecular mechanisms for adaptive tolerance and other T cell  
663 anergy models. *Seminars in immunology* 19:140-152.
- 664 Cuenca, A., F. Cheng, H. Wang, J. Brayer, P. Horna, L. Gu, H. Bien, I.M. Borrello, H.I. Levitsky, and  
665 E.M. Sotomayor. 2003. Extra-lymphatic solid tumor growth is not immunologically  
666 ignored and results in early induction of antigen-specific T-cell anergy: dominant role of  
667 cross-tolerance to tumor antigens. *Cancer research* 63:9007-9015.
- 668 DL, K.L.a.M. 2017. Relationship between CD4 Regulatory T Cells and Anergy In Vivo. *Journal of*  
669 *immunology (Baltimore, Md. : 1950)* 198:2527.
- 670 Dobin, A., C.A. Davis, F. Schlesinger, J. Drenkow, C. Zaleski, S. Jha, P. Batut, M. Chaisson, and  
671 T.R. Gingeras. 2013. STAR: ultrafast universal RNA-seq aligner. *Bioinformatics* 29:15-21.



- 672 Dvorak, V., T. Wiedmer, A. Ingles-Prieto, P. Altermatt, H. Batoulis, F. Bärenz, E. Bender, D.  
673 Digles, F. Dürrenberger, L.H. Heitman, I.J. AP, D.B. Kell, S. Kicking, D. Körzö, P. Leippe,  
674 T. Licher, V. Manolova, R. Rizzetto, F. Sassone, L. Scarabottolo, A. Schlessinger, V.  
675 Schneider, H.J. Sijben, A.L. Steck, H. Sundström, S. Tremolada, M. Wilhelm, M. Wright  
676 Muelas, D. Zindel, C.M. Steppan, and G. Superti-Furga. 2021. An Overview of Cell-Based  
677 Assay Platforms for the Solute Carrier Family of Transporters. *Frontiers in pharmacology*  
678 12:722889.
- 679 ElTanbouly, M.A., and R.J. Noelle. 2021. Rethinking peripheral T cell tolerance: checkpoints  
680 across a T cell's journey. *Nat Rev Immunol* 21:257-267.
- 681 Emmons-Bell, M., and I.K. Hariharan. 2021. Membrane potential regulates Hedgehog signalling  
682 in the *Drosophila* wing imaginal disc. *EMBO reports* 22:e51861.
- 683 Feng, Y., A. Arvey, T. Chinen, J. van der Veecken, G. Gasteiger, and A.Y. Rudensky. 2014. Control  
684 of the inheritance of regulatory T cell identity by a cis element in the *Foxp3* locus. *Cell*  
685 158:749-763.
- 686 Floess, S., J. Freyer, C. Siewert, U. Baron, S. Olek, J. Polansky, K. Schlawe, H.D. Chang, T. Bopp, E.  
687 Schmitt, S. Klein-Hessling, E. Serfling, A. Hamann, and J. Huehn. 2007. Epigenetic control  
688 of the *foxp3* locus in regulatory T cells. *PLoS biology* 5:e38.
- 689 Fujino, T., J.H. Leslie, R. Eavri, J.L. Chen, W.C. Lin, G.H. Flanders, E. Borok, T.L. Horvath, and E.  
690 Nedivi. 2011. CPG15 regulates synapse stability in the developing and adult brain. *Genes*  
691 *& development* 25:2674-2685.
- 692 Geltink, R.I.K., R.L. Kyle, and E.L. Pearce. 2018. Unraveling the Complex Interplay Between T Cell  
693 Metabolism and Function. *Annual review of immunology* 36:461-488.
- 694 Gonzalez-Figueroa, P., J.A. Roco, I. Papa, L. Núñez Villacís, M. Stanley, M.A. Linterman, A. Dent,  
695 P.F. Canete, and C.G. Vinuesa. 2021. Follicular regulatory T cells produce neuritin to  
696 regulate B cells. *Cell*
- 697 Hamill, M.J., R. Afeyan, M.V. Chakravarthy, and T. Tramontin. 2020. Endogenous Metabolic  
698 Modulators: Emerging Therapeutic Potential of Amino Acids. *iScience* 23:101628.
- 699 Huang, C.T., D.L. Huso, Z. Lu, T. Wang, G. Zhou, E.P. Kennedy, C.G. Drake, D.J. Morgan, L.A.  
700 Sherman, A.D. Higgins, D.M. Pardoll, and A.J. Adler. 2003. CD4<sup>+</sup> T cells pass through an  
701 effector phase during the process of in vivo tolerance induction. *Journal of immunology*  
702 (*Baltimore, Md. : 1950*) 170:3945-3953.
- 703 Huang, C.T., C.J. Workman, D. Flies, X. Pan, A.L. Marson, G. Zhou, E.L. Hipkiss, S. Ravi, J.  
704 Kowalski, H.I. Levitsky, J.D. Powell, D.M. Pardoll, C.G. Drake, and D.A. Vignali. 2004. Role  
705 of LAG-3 in regulatory T cells. *Immunity* 21:503-513.
- 706 Javaherian, A., and H.T. Cline. 2005. Coordinated motor neuron axon growth and  
707 neuromuscular synaptogenesis are promoted by CPG15 in vivo. *Neuron* 45:505-512.
- 708 Joesch, C., E. Guevarra, S.P. Parel, A. Bergner, P. Zbinden, D. Konrad, and H. Albrecht. 2008. Use  
709 of FLIPR membrane potential dyes for validation of high-throughput screening with the  
710 FLIPR and microARCS technologies: identification of ion channel modulators acting on  
711 the GABA(A) receptor. *J Biomol Screen* 13:218-228.
- 712 Kalekar, L.A., S.E. Schmiel, S.L. Nandiwada, W.Y. Lam, L.O. Barsness, N. Zhang, G.L. Stritesky, D.  
713 Malhotra, K.E. Pauken, J.L. Linehan, M.G. O'Sullivan, B.T. Fife, K.A. Hogquist, M.K.  
714 Jenkins, and D.L. Mueller. 2016. CD4(+) T cell anergy prevents autoimmunity and  
715 generates regulatory T cell precursors. *Nature immunology* 17:304-314.

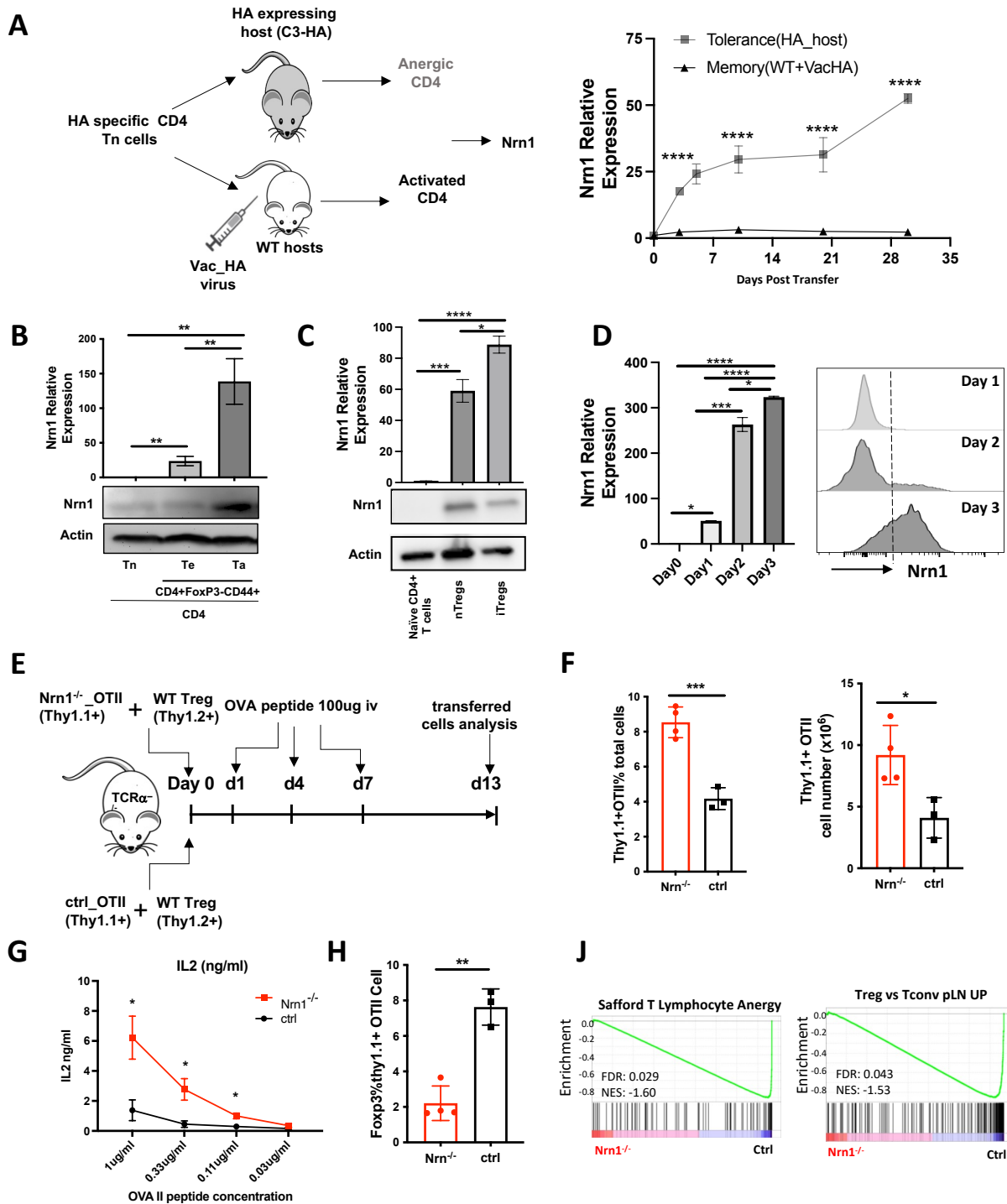


- 716 Kiefer, H., A.J. Blume, and H.R. Kaback. 1980. Membrane potential changes during mitogenic  
717 stimulation of mouse spleen lymphocytes. *Proceedings of the National Academy of*  
718 *Sciences of the United States of America* 77:2200-2204.
- 719 Kim, J.M., J.P. Rasmussen, and A.Y. Rudensky. 2007. Regulatory T cells prevent catastrophic  
720 autoimmunity throughout the lifespan of mice. *Nature immunology* 8:191-197.
- 721 Kuczma, M.P., E.A. Szurek, A. Cebula, V.L. Ngo, M. Pietrzak, P. Kraj, T.L. Denning, and L.  
722 Ignatowicz. 2021. Self and microbiota-derived epitopes induce CD4(+) T cell anergy and  
723 conversion into CD4(+)Foxp3(+) regulatory cells. *Mucosal Immunol* 14:443-454.
- 724 Levin, M. 2021. Bioelectric signaling: Reprogrammable circuits underlying embryogenesis,  
725 regeneration, and cancer. *Cell* 184:1971-1989.
- 726 Li, X., Y. Liang, M. LeBlanc, C. Benner, and Y. Zheng. 2014. Function of a Foxp3 cis-element in  
727 protecting regulatory T cell identity. *Cell* 158:734-748.
- 728 Lim, D.G., Y.H. Park, S.E. Kim, S.H. Jeong, and S.C. Kim. 2013. Diagnostic value of tolerance-  
729 related gene expression measured in the recipient alloantigen-reactive T cell fraction.  
730 *Clinical immunology (Orlando, Fla.)* 148:219-226.
- 731 Liu, G.Y., and D.M. Sabatini. 2020. mTOR at the nexus of nutrition, growth, ageing and disease.  
732 *Nat Rev Mol Cell Biol* 21:183-203.
- 733 Long, L., J. Wei, S.A. Lim, J.L. Raynor, H. Shi, J.P. Connelly, H. Wang, C. Guy, B. Xie, N.M.  
734 Chapman, G. Fu, Y. Wang, H. Huang, W. Su, J. Saravia, I. Risch, Y.D. Wang, Y. Li, M. Niu, Y.  
735 Dhungana, A. Kc, P. Zhou, P. Vogel, J. Yu, S.M. Pruett-Miller, J. Peng, and H. Chi. 2021.  
736 CRISPR screens unveil signal hubs for nutrient licensing of T cell immunity. *Nature*  
737 600:308-313.
- 738 Love, M.I., W. Huber, and S. Anders. 2014. Moderated estimation of fold change and dispersion  
739 for RNA-seq data with DESeq2. *Genome biology* 15:550.
- 740 Ma, Y., K. Poole, J. Goyette, and K. Gaus. 2017. Introducing Membrane Charge and Membrane  
741 Potential to T Cell Signaling. *Frontiers in immunology* 8:1513.
- 742 Martinez, R.J., N. Zhang, S.R. Thomas, S.L. Nandiwada, M.K. Jenkins, B.A. Binstadt, and D.L.  
743 Mueller. 2012. Arthritogenic self-reactive CD4+ T cells acquire an FR4hiCD73hi anergic  
744 state in the presence of Foxp3+ regulatory T cells. *Journal of immunology (Baltimore,*  
745 *Md. : 1950)* 188:170-181.
- 746 McNearney, T., B.A. Baethge, S. Cao, R. Alam, J.R. Lisse, and K.N. Westlund. 2004. Excitatory  
747 amino acids, TNF-alpha, and chemokine levels in synovial fluids of patients with active  
748 arthropathies. *Clinical and experimental immunology* 137:621-627.
- 749 Mercadante, E.R., and U.M. Lorenz. 2016. Breaking Free of Control: How Conventional T Cells  
750 Overcome Regulatory T Cell Suppression. *Frontiers in immunology* 7:193.
- 751 Miller, S.D., W.J. Karpus, and T.S. Davidson. 2007. Experimental Autoimmune Encephalomyelitis  
752 in the Mouse. *Current protocols in immunology* CHAPTER:Unit-15 11.
- 753 Monroe, J.G., and J.C. Cambier. 1983. B cell activation. I. Anti-immunoglobulin-induced receptor  
754 cross-linking results in a decrease in the plasma membrane potential of murine B  
755 lymphocytes. *The Journal of experimental medicine* 157:2073-2086.
- 756 Nedivi, E., G.Y. Wu, and H.T. Cline. 1998. Promotion of dendritic growth by CPG15, an activity-  
757 induced signaling molecule. *Science (New York, N.Y.)* 281:1863-1866.

- 758 Nik, A.M., B. Pressly, V. Singh, S. Antrobus, S. Hulsizer, M.A. Rogawski, H. Wulff, and I.N. Pessah.  
759 2017. Rapid Throughput Analysis of GABA(A) Receptor Subtype Modulators and Blockers  
760 Using DiSBAC(1)(3) Membrane Potential Red Dye. *Mol Pharmacol* 92:88-99.
- 761 Nystrom, S.N., D. Bourges, S. Garry, E.M. Ross, I.R. van Driel, and P.A. Gleeson. 2014. Transient  
762 Treg-cell depletion in adult mice results in persistent self-reactive CD4(+) T-cell  
763 responses. *European journal of immunology* 44:3621-3631.
- 764 Olenchock, B.A., J.C. Rathmell, and M.G. Vander Heiden. 2017. Biochemical Underpinnings of  
765 Immune Cell Metabolic Phenotypes. *Immunity* 46:703-713.
- 766 Opejin, A., A. Surnov, Z. Misulovin, M. Pherson, C. Gross, C.A. Iberg, I. Fallahee, J. Bourque, D.  
767 Dorsett, and D. Hawiger. 2020. A Two-Step Process of Effector Programming Governs  
768 CD4(+) T Cell Fate Determination Induced by Antigenic Activation in the Steady State.  
769 *Cell reports* 33:108424.
- 770 Pandya, N.J., C. Seeger, N. Babai, M.A. Gonzalez-Lozano, V. Mack, J.C. Lodder, Y. Gouwenberg,  
771 H.D. Mansvelder, U.H. Danielson, K.W. Li, M. Heine, S. Spijker, R. Frischknecht, and A.B.  
772 Smit. 2018. Noelin1 Affects Lateral Mobility of Synaptic AMPA Receptors. *Cell reports*  
773 24:1218-1230.
- 774 Peng, M., and M.O. Li. 2023. Metabolism along the life journey of T cells. *Life Metab* 2:  
775 Plitas, G., C. Konopacki, K. Wu, P.D. Bos, M. Morrow, E.V. Putintseva, D.M. Chudakov, and A.Y.  
776 Rudensky. 2016. Regulatory T Cells Exhibit Distinct Features in Human Breast Cancer.  
777 *Immunity* 45:1122-1134.
- 778 Putz, U., C. Harwell, and E. Nedivi. 2005. Soluble CPG15 expressed during early development  
779 rescues cortical progenitors from apoptosis. *Nature neuroscience* 8:322-331.
- 780 Ramirez, G.A., L.A. Coletto, C. Sciorati, E.P. Bozzolo, P. Manunta, P. Rovere-Querini, and A.A.  
781 Manfredi. 2018. Ion Channels and Transporters in Inflammation: Special Focus on TRP  
782 Channels and TRPC6. *Cells* 7:
- 783 Safford, M., S. Collins, M.A. Lutz, A. Allen, C.T. Huang, J. Kowalski, A. Blackford, M.R. Horton, C.  
784 Drake, R.H. Schwartz, and J.D. Powell. 2005. Egr-2 and Egr-3 are negative regulators of T  
785 cell activation. *Nature immunology* 6:472-480.
- 786 Salmond, R.J. 2018. mTOR Regulation of Glycolytic Metabolism in T Cells. *Frontiers in cell and*  
787 *developmental biology* 6:122.
- 788 Saravia, J., J.L. Raynor, N.M. Chapman, S.A. Lim, and H. Chi. 2020. Signaling networks in  
789 immunometabolism. *Cell research* 30:328-342.
- 790 Sarchielli, P., M. Di Filippo, A. Candelieri, D. Chiasserini, A. Mattioni, S. Tenaglia, M. Bonucci,  
791 and P. Calabresi. 2007. Expression of ionotropic glutamate receptor GLUR3 and effects  
792 of glutamate on MBP- and MOG-specific lymphocyte activation and chemotactic  
793 migration in multiple sclerosis patients. *Journal of neuroimmunology* 188:146-158.
- 794 Schietinger, A., J.J. Delrow, R.S. Basom, J.N. Blattman, and P.D. Greenberg. 2012. Rescued  
795 tolerant CD8 T cells are preprogrammed to reestablish the tolerant state. *Science (New*  
796 *York, N.Y.)* 335:723-727.
- 797 Schietinger, A., M. Philip, V.E. Krisnawan, E.Y. Chiu, J.J. Delrow, R.S. Basom, P. Lauer, D.G.  
798 Brockstedt, S.E. Knoblaugh, G.J. Hammerling, T.D. Schell, N. Garbi, and P.D. Greenberg.  
799 2016. Tumor-Specific T Cell Dysfunction Is a Dynamic Antigen-Driven Differentiation  
800 Program Initiated Early during Tumorigenesis. *Immunity* 45:389-401.

- 801 Schwenk, J., N. Harmel, A. Brechet, G. Zolles, H. Berkefeld, C.S. Muller, W. Bildl, D. Baehrens, B.  
802 Huber, A. Kulik, N. Klocker, U. Schulte, and B. Fakler. 2012. High-resolution proteomics  
803 unravel architecture and molecular diversity of native AMPA receptor complexes.  
804 *Neuron* 74:621-633.
- 805 Shannon, P., A. Markiel, O. Ozier, N.S. Baliga, J.T. Wang, D. Ramage, N. Amin, B. Schwikowski,  
806 and T. Ideker. 2003. Cytoscape: a software environment for integrated models of  
807 biomolecular interaction networks. *Genome Res* 13:2498-2504.
- 808 Shimada, T., T. Yoshida, and K. Yamagata. 2016. Neuritin Mediates Activity-Dependent Axonal  
809 Branch Formation in Part via FGF Signaling. *The Journal of neuroscience : the official*  
810 *journal of the Society for Neuroscience* 36:4534-4548.
- 811 Shin, D.S., A. Jordan, S. Basu, R.M. Thomas, S. Bandyopadhyay, E.F. de Zoeten, A.D. Wells, and F.  
812 Macian. 2014. Regulatory T cells suppress CD4+ T cells through NFAT-dependent  
813 transcriptional mechanisms. *EMBO reports* 15:991-999.
- 814 Silva Morales, M., and D. Mueller. 2018. Anergy into T regulatory cells: an integration of  
815 metabolic cues and epigenetic changes at the Foxp3 conserved non-coding sequence 2.  
816 *F1000Research* 7:
- 817 Sinclair, L.V., J. Rolf, E. Emslie, Y.B. Shi, P.M. Taylor, and D.A. Cantrell. 2013. Control of amino-  
818 acid transport by antigen receptors coordinates the metabolic reprogramming essential  
819 for T cell differentiation. *Nature immunology* 14:500-508.
- 820 Singer, M., C. Wang, L. Cong, N.D. Marjanovic, M.S. Kowalczyk, H. Zhang, J. Nyman, K. Sakuishi,  
821 S. Kurtulus, D. Gennert, J. Xia, J.Y. Kwon, J. Nevin, R.H. Herbst, I. Yanai, O. Rozenblatt-  
822 Rosen, V.K. Kuchroo, A. Regev, and A.C. Anderson. 2016. A Distinct Gene Module for  
823 Dysfunction Uncoupled from Activation in Tumor-Infiltrating T Cells. *Cell* 166:1500-  
824 1511.e1509.
- 825 Subramanian, A., P. Tamayo, V.K. Mootha, S. Mukherjee, B.L. Ebert, M.A. Gillette, A. Paulovich,  
826 S.L. Pomeroy, T.R. Golub, E.S. Lander, and J.P. Mesirov. 2005. Gene set enrichment  
827 analysis: a knowledge-based approach for interpreting genome-wide expression  
828 profiles. *Proceedings of the National Academy of Sciences of the United States of*  
829 *America* 102:15545-15550.
- 830 Subramanian, J., K. Michel, M. Benoit, and E. Nedivi. 2019. CPG15/Neuritin Mimics Experience  
831 in Selecting Excitatory Synapses for Stabilization by Facilitating PSD95 Recruitment. *Cell*  
832 *reports* 28:1584-1595.e1585.
- 833 Sullivan, M.R., L.V. Danai, C.A. Lewis, S.H. Chan, D.Y. Gui, T. Kunchok, E.A. Dennstedt, M.G.  
834 Vander Heiden, and A. Muir. 2019. Quantification of microenvironmental metabolites in  
835 murine cancers reveals determinants of tumor nutrient availability. *eLife* 8:
- 836 Sundelacruz, S., M. Levin, and D.L. Kaplan. 2009. Role of membrane potential in the regulation  
837 of cell proliferation and differentiation. *Stem Cell Rev Rep* 5:231-246.
- 838 Vahl, J.C., C. Drees, K. Heger, S. Heink, J.C. Fischer, J. Nedjic, N. Ohkura, H. Morikawa, H. Poeck,  
839 S. Schallenberg, D. Riess, M.Y. Hein, T. Buch, B. Polic, A. Schonle, R. Zeiser, A. Schmitt-  
840 Graff, K. Kretschmer, L. Klein, T. Korn, S. Sakaguchi, and M. Schmidt-Supprian. 2014.  
841 Continuous T cell receptor signals maintain a functional regulatory T cell pool. *Immunity*  
842 41:722-736.

- 843 Vanasek, T.L., S.L. Nandiwada, M.K. Jenkins, and D.L. Mueller. 2006. CD25+Foxp3+ regulatory T  
844 cells facilitate CD4+ T cell clonal anergy induction during the recovery from  
845 lymphopenia. *Journal of immunology (Baltimore, Md. : 1950)* 176:5880-5889.
- 846 Wang, Y., A. Tao, M. Vaeth, and S. Feske. 2020. Calcium regulation of T cell metabolism. *Current*  
847 *opinion in physiology* 17:207-223.
- 848 Whiteaker, K.L., S.M. Gopalakrishnan, D. Groebe, C.C. Shieh, U. Warrior, D.J. Burns, M.J.  
849 Coghlan, V.E. Scott, and M. Gopalakrishnan. 2001. Validation of FLIPR membrane  
850 potential dye for high throughput screening of potassium channel modulators. *J Biomol*  
851 *Screen* 6:305-312.
- 852 Workman, C.J., L.W. Collison, M. Bettini, M.R. Pillai, J.E. Rehg, and D.A. Vignali. 2011. In vivo  
853 Treg suppression assays. *Methods in molecular biology (Clifton, N.J.)* 707:119-156.
- 854 Yao, J.J., X.F. Gao, C.W. Chow, X.Q. Zhan, C.L. Hu, and Y.A. Mei. 2012. Neuritin activates insulin  
855 receptor pathway to up-regulate Kv4.2-mediated transient outward K<sup>+</sup> current in rat  
856 cerebellar granule neurons. *The Journal of biological chemistry* 287:41534-41545.
- 857 Yu, W., Z. Wang, X. Yu, Y. Zhao, Z. Xie, K. Zhang, Z. Chi, S. Chen, T. Xu, D. Jiang, X. Guo, M. Li, J.  
858 Zhang, H. Fang, D. Yang, Y. Guo, X. Yang, X. Zhang, Y. Wu, W. Yang, and D. Wang. 2022.  
859 Kir2.1-mediated membrane potential promotes nutrient acquisition and inflammation  
860 through regulation of nutrient transporters. *Nature communications* 13:3544.
- 861 Zha, Y., R. Marks, A.W. Ho, A.C. Peterson, S. Janardhan, I. Brown, K. Praveen, S. Stang, J.C.  
862 Stone, and T.F. Gajewski. 2006. T cell anergy is reversed by active Ras and is regulated  
863 by diacylglycerol kinase- $\alpha$ . *Nature immunology* 7:1166-1173.
- 864 Zheng, Y., G.M. Delgoffe, C.F. Meyer, W. Chan, and J.D. Powell. 2009. Anergic T cells are  
865 metabolically anergic. *Journal of immunology (Baltimore, Md. : 1950)* 183:6095-6101.
- 866 Zheng, Y., S. Josefowicz, A. Chaudhry, X.P. Peng, K. Forbush, and A.Y. Rudensky. 2010. Role of  
867 conserved non-coding DNA elements in the Foxp3 gene in regulatory T-cell fate. *Nature*  
868 463:808-812.
- 869 Zhou, S., and J. Zhou. 2014. Neuritin, a neurotrophic factor in nervous system physiology.  
870 *Current medicinal chemistry* 21:1212-1219.
- 871 Zhou, Y., C.O. Wong, K.J. Cho, D. van der Hoeven, H. Liang, D.P. Thakur, J. Luo, M. Babic, K.E.  
872 Zinsmaier, M.X. Zhu, H. Hu, K. Venkatachalam, and J.F. Hancock. 2015. SIGNAL  
873 TRANSDUCTION. Membrane potential modulates plasma membrane phospholipid  
874 dynamics and K-Ras signaling. *Science (New York, N.Y.)* 349:873-876.
- 875 Zito, A., D. Cartelli, G. Cappelletti, A. Cariboni, W. Andrews, J. Parnavelas, A. Poletti, and M.  
876 Galbiati. 2014. Neuritin 1 promotes neuronal migration. *Brain Structure and Function*  
877 219:105-118.
- 878
- 879
- 880
- 881
- 882
- 883



885

886 **Figure 1. Nrn1 expression and function in anergic T cells.**

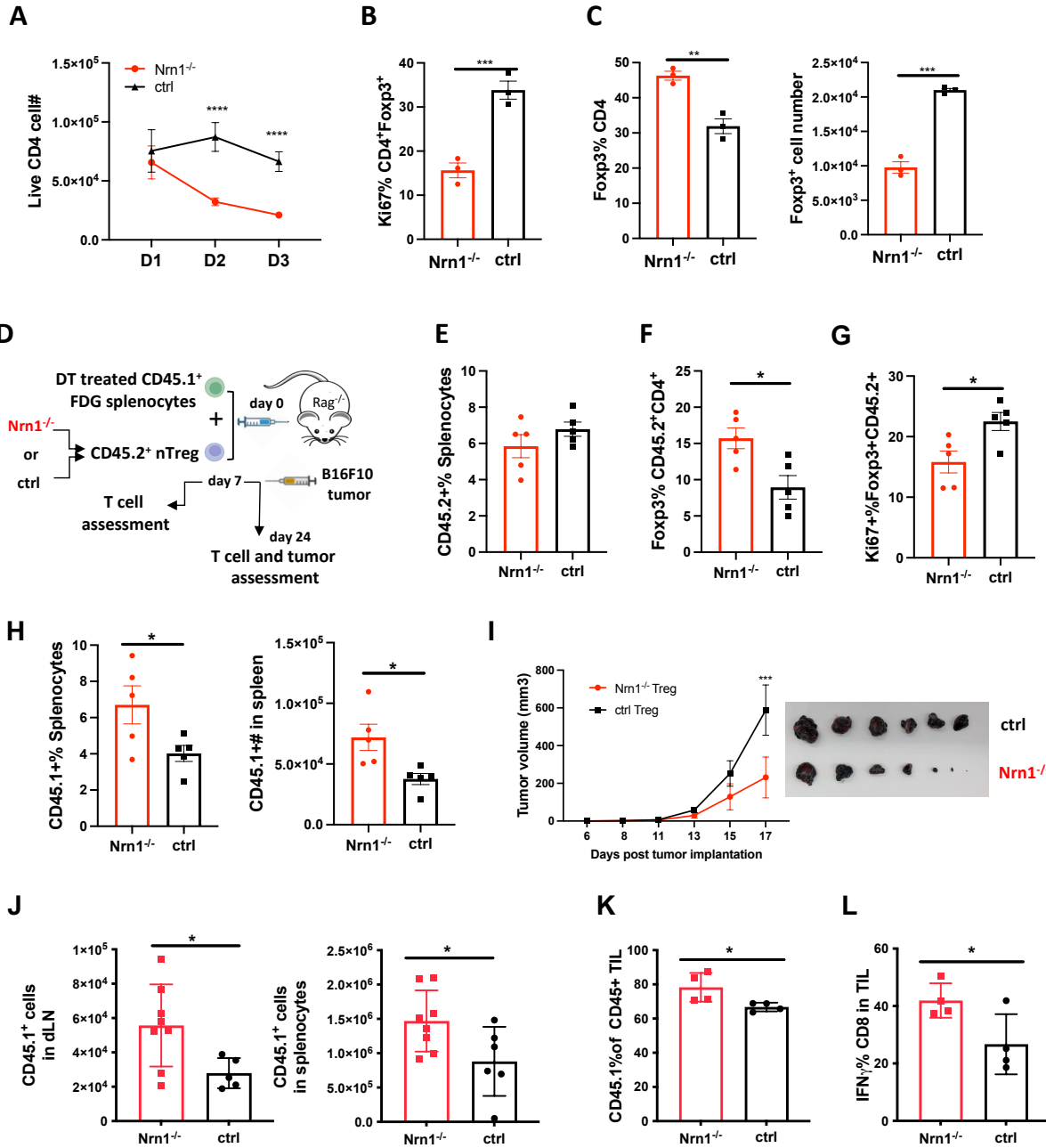
887 (A) Experimental scheme identifying Nrn1 in anergic T cells and qRT-PCR confirmation of Nrn1  
 888 expression in HA-specific CD4 cells recovered from HA-expressing host vs WT host activated  
 889 with Vac\_HA virus. (B) qRT-PCR and western blot detecting Nrn1 expression in naïve

890 CD4<sup>+</sup>CD62L<sup>hi</sup>CD44<sup>lo</sup> Tn cell, CD4<sup>+</sup>Foxp3<sup>-</sup>CD44<sup>hi</sup>CD73<sup>-</sup>FR<sup>-</sup> Te cells and CD4<sup>+</sup>Foxp3<sup>-</sup>  
891 CD44<sup>hi</sup>CD73<sup>+</sup>FR<sup>+</sup> Ta cells. (C) Nrn1 expression was measured by qRT-PCR and western blot  
892 among naïve CD4<sup>+</sup> T cells, CD4<sup>+</sup>Foxp3<sup>+</sup> nTreg, and *in vitro* generated iTregs. (D) Nrn1 expression  
893 was detected by qRT-PCR and flow cytometry among naïve CD4<sup>+</sup> cells and activated CD4<sup>+</sup> cells  
894 on days 1, 2, and 3 after activation. qPCR Data are presented as average  $\pm$  SEM. \*p<0.05,  
895 \*\*p<0.01, \*\*\*p<0.001, \*\*\*\*p<0.0001. Triplicates were used. Ordinary one-way ANOVA was  
896 performed for multi-comparison.

897 (E-J). Anergy induction *in vivo*. (E) Experimental outline evaluating anergy development *in vivo*:  
898 2x10<sup>6</sup> Thy1.1<sup>+</sup> Nrn1<sup>-/-</sup> or ctrl CD4 OTII T cells were co-transferred with 5x10<sup>5</sup> Thy1.2<sup>+</sup>Thy1.1<sup>-</sup>  
899 WT Treg cells into TCR $\alpha$ <sup>-/-</sup> mice. Cells were recovered on day 13 post-transfer. (F) Proportions  
900 and numbers of OTII cells recovered from recipient spleen; (G) IL2 secretion from OTII cells  
901 upon *ex vivo* stimulation with OVA peptide. (H) Foxp3<sup>+</sup> cell proportion among Thy1.1<sup>+</sup> Nrn1<sup>-/-</sup> or  
902 ctrl CD4 cells. (I & J) Nrn1<sup>-/-</sup> vs ctrl OTII cells recovered from the peptide-induced anergy model  
903 were subjected to bulk RNASeq analysis. GSEA comparing the expression of signature genes for  
904 anergy (I) and Treg (J) among ctrl and Nrn1<sup>-/-</sup> OTII cells.

905 Data are presented as mean  $\pm$ SEM and representative of 3 independent experiments (N $\geq$ 4 mice  
906 per group). \*p<0.05, \*\*p<0.01, \*\*\*p<0.001. Unpaired Student's t-tests were performed.

907



908

909 **Figure 2. Reduced proliferation and suppression function in Nrn1<sup>-/-</sup> Treg cells.**

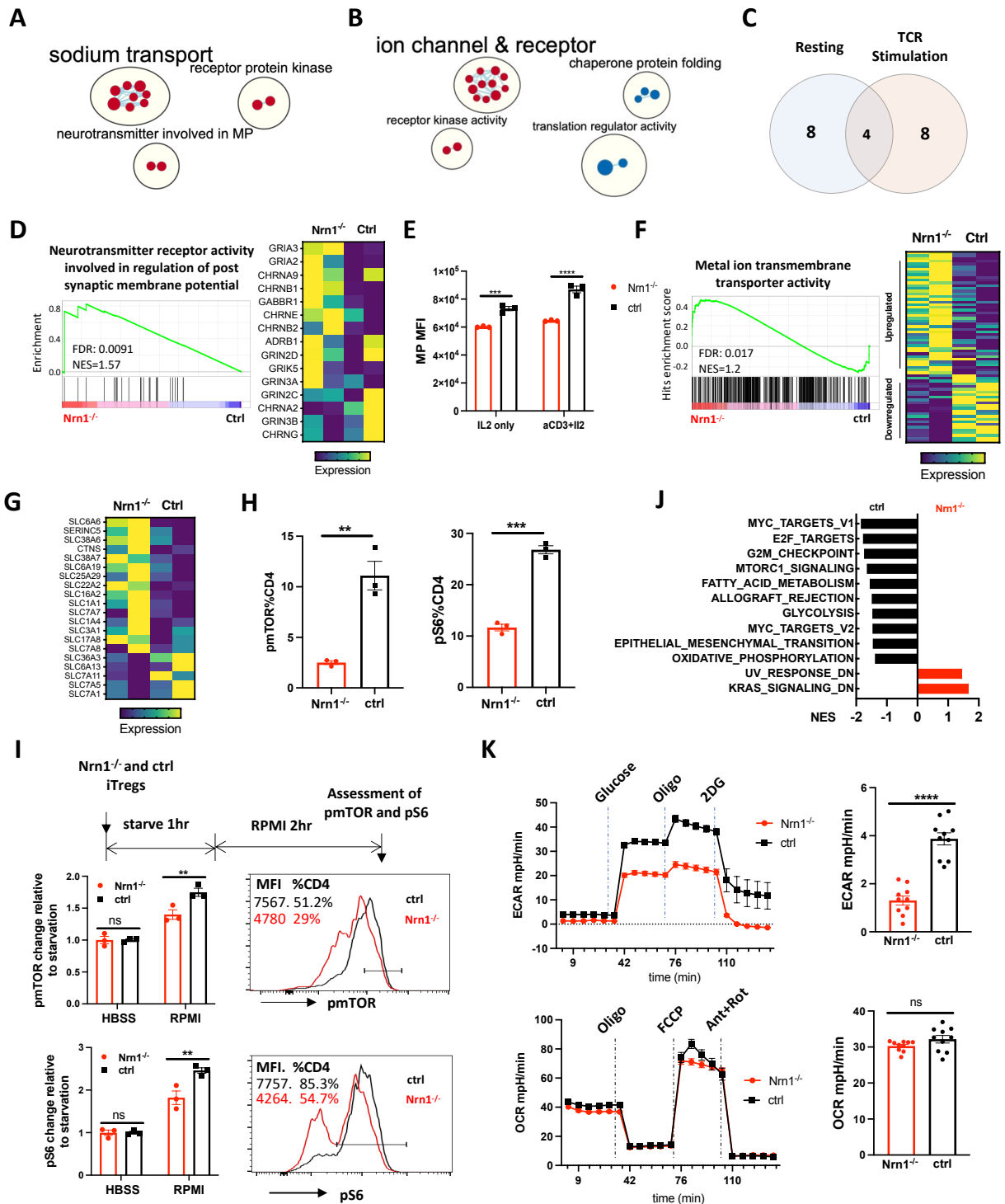
910 (A-C) iTreg cell expansion after restimulation. (A) The number of live cells from day 1 to day 3  
 911 after iTreg cell restimulation with anti-CD3. (B) Ki67 expression among CD4<sup>+</sup>Foxp3<sup>+</sup> cells day 3  
 912 after restimulation. (C) Foxp3<sup>+</sup> cell proportion and number among live CD4<sup>+</sup> cells day 3 after  
 913 restimulation. Triplicates in each experiment, data represent one of four independent experiments.  
 914 (D-L). Nrn1<sup>-/-</sup> or ctrl nTreg cells expansion and suppression *in vivo*. (D) The experimental scheme.  
 915 CD45.2<sup>+</sup> nTreg T cells from Nrn1<sup>-/-</sup> or ctrl were transferred with CD45.1<sup>+</sup> FDG splenocytes devoid



916 of Tregs into Rag2<sup>-/-</sup> host. Treg cell expansion and suppression toward FDG CD45.1<sup>+</sup> responder  
917 cells were evaluated on day 7 post cell transfer. Alternatively, B16F10 tumor cells were inoculated  
918 on day 7 after cell transfer and monitored for tumor growth. **(E-H)** CD45.2<sup>+</sup> cell proportion **(E)**,  
919 Foxp3 retention **(F)**, and Ki67 expression among Foxp3<sup>+</sup> cells **(G)** at day 7 post cell transfer. **(H)**  
920 CD45.1<sup>+</sup> cell proportion and number in the spleen of Nrn1<sup>-/-</sup> or ctrl Treg hosts day 7 post cell  
921 transfer. **(I-L)**. Treg cell suppression toward anti-tumor response. **(I)** Tumor growth curve and  
922 tumor size at harvest from Nrn1<sup>-/-</sup> or ctrl nTreg hosts. **(J)** CD45.1<sup>+</sup> cell count in tumor draining  
923 lymph node (LN) and spleen. **(K)** the proportion of CD45.1<sup>+</sup> cells among CD45<sup>+</sup> tumor  
924 lymphocyte infiltrates (TILs). **(L)** IFN $\gamma$ % among CD8<sup>+</sup> T cells in TILs. n $\geq$ 5 mice per group. **(E-**  
925 **H)** represents three independent experiments, **(I-L)** represents two independent experiments. Data  
926 are presented as mean  $\pm$ SEM \*p<0.05, \*\*p<0.01, \*\*\*p<0.001, \*\*\*\*p<0.0001. Unpaired Student's  
927 t-tests were performed.

928

929



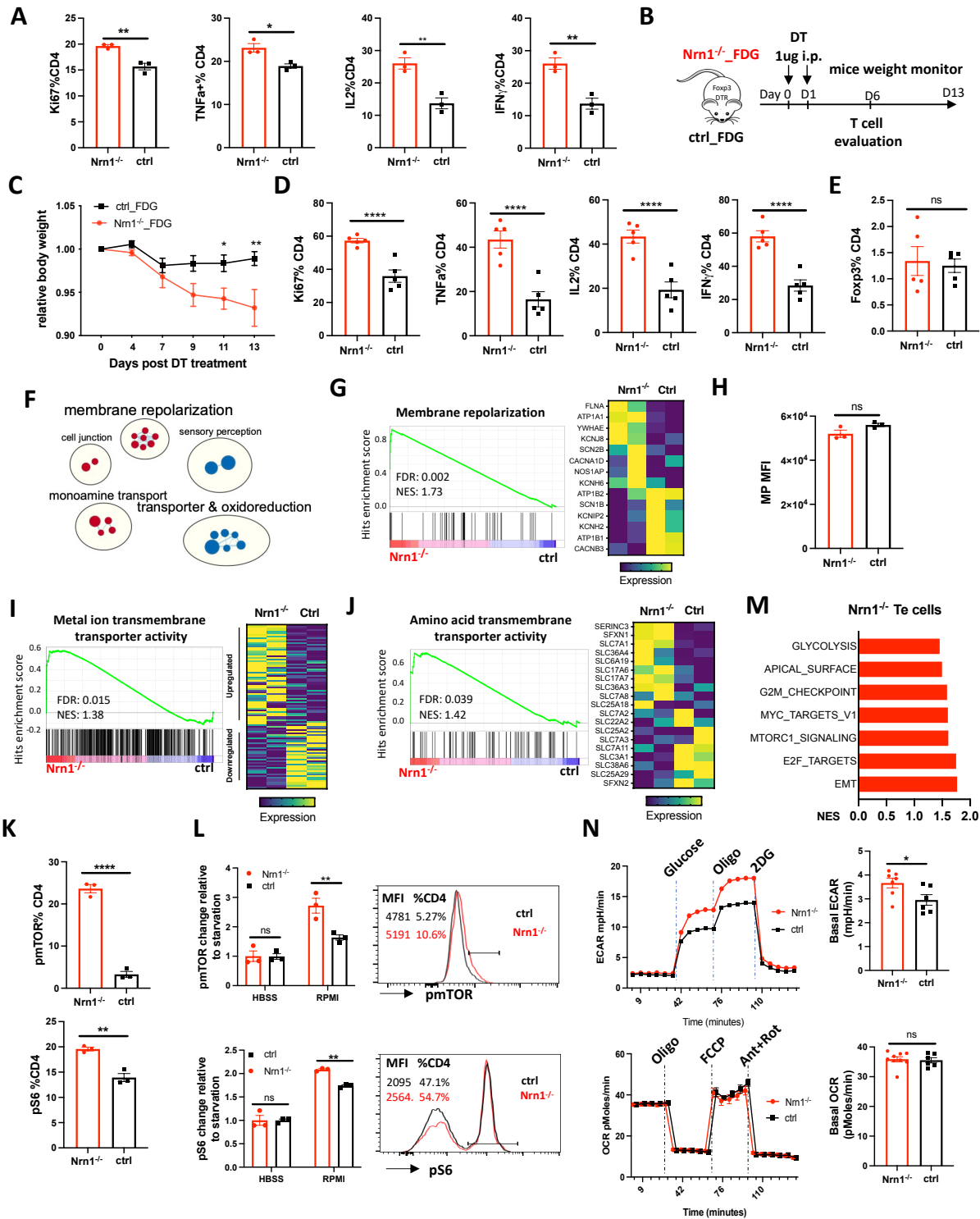
930

931 **Figure 3. Nrn1 expression impacts Treg cell electrical and metabolic state.**

932 (A-C). Gene sets clusters enriched in Nrn1<sup>-/-</sup> and ctrl iTreg cells. Gene sets cluster analysis via  
 933 Cytoscape was performed on Gene ontology Molecular Function (GO\_MF) gene sets. The results  
 934 cutoff: p-value ≤0.05 and FDR q-value ≤0.1. (A) Gene sets cluster in Nrn1<sup>-/-</sup> iTreg cells cultured

935 under resting condition (IL2 only) (Figure 3-figure supplement Table 1). **(B)** Gene sets clusters in  
936 *Nrn1*<sup>-/-</sup> and ctrl iTreg cells reactivated with anti-CD3 (Figure 3-figure supplement Table 2). **(C)**  
937 Comparison of enriched gene sets in *Nrn1*<sup>-/-</sup> under resting vs. activating condition (Figure 3-figure  
938 supplement Table 3). **(D-F)** Changes relating to cell electric state. **(D)** Enrichment of  
939 “GOMF\_Neurotransmitter receptor activity involved in the regulation of postsynaptic membrane  
940 potential” gene set and enriched gene expression heatmap. **(E)** Membrane potential was measured  
941 in *Nrn1*<sup>-/-</sup> and ctrl iTreg cells cultured in IL2 or activated with anti-CD3 in the presence of IL2.  
942 Data represent three independent experiments. **(F)** Enrichment of “GOMF\_Metal ion  
943 transmembrane transporter activity” gene set and enriched gene expression heatmap (Figure 3-  
944 figure supplement 1A). **(G-K)**. Metabolic changes associated with *Nrn1*<sup>-/-</sup> iTreg. **(G)** Heatmap of  
945 differentially expressed amino acid (AA) transport-related genes (from “MF\_Amino acid  
946 transmembrane transporter activity” gene list) in *Nrn1*<sup>-/-</sup> and ctrl iTreg cells. **(H)** pmTOR and pS6  
947 levels in TCR activated iTreg cells measured by flow cytometry. n=3 replicates per group. Data  
948 represent three independent experiments. **(I)** Measurement of pmTOR and pS6 in iTreg cells that  
949 were deprived of nutrients for 1h and refed with RPMI for two hours. **(J)** Hallmark gene sets  
950 significantly enriched in *Nrn1*<sup>-/-</sup> and ctrl iTreg. NOM p-val<0.05, FDR q-val<0.25. **(K)** Seahorse  
951 analysis of extracellular acidification rate (ECAR) and oxygen consumption rate (OCR) in *Nrn1*<sup>-/-</sup>  
952 and ctrl iTreg cells. n=6~10 technical replicates per group. Data represent three independent  
953 experiments. \*\*p<0.01, \*\*\*p<0.001, \*\*\*\*p<0.0001. Unpaired student t-test for two-group  
954 comparison. Unpaired t-test (H, K), two-way ANOVA (E, I). ns, not significant.

955



956

957 **Figure 4. Nrn1 deficiency affects Te cell response.**

958 (A) Comparison of cell proliferation and cytokine expression in Nrn1<sup>-/-</sup> and ctrl Te cells. Data

959 represent one of three independent experiments. (B-E) An enhanced autoimmune response in

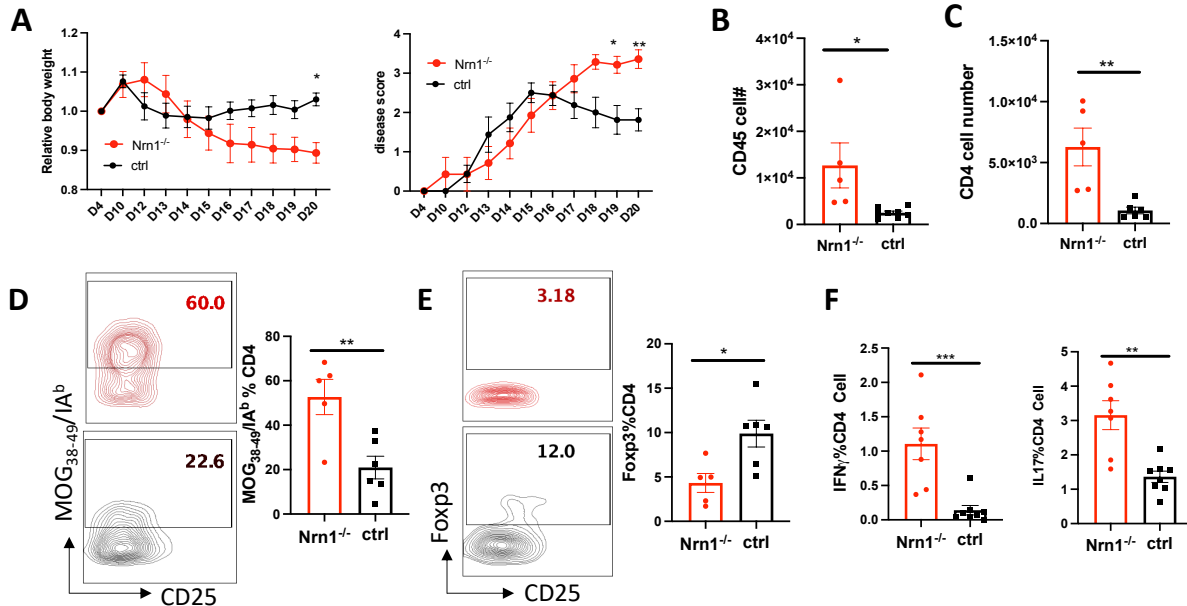
960 Nrn1<sup>-/-</sup> mice *in vivo*. (B) Experimental scheme. Nrn1<sup>-/-</sup> mice were crossed with FDG and

961 *Nrn1*<sup>-/-</sup>\_FDG or ctrl\_FDG mice were obtained. The autoimmune response was induced by  
962 injecting DT i.p. to delete endogenous Treg cells. Mice's weight change was monitored after  
963 disease induction. (C) Relative body weight change after autoimmune response induction. (D)  
964 Mice were harvested 6 days after DT injection and assessed for ki67, cytokine TNF $\alpha$ , IL2, and  
965 IFN $\gamma$  expression in CD4<sup>+</sup> cells. (E) Foxp3 expression among CD4<sup>+</sup> cells day 6 post DT treatment.  
966 n $\geq$ 5 mice per group. Data represent four independent experiments. (F-I) Changes relating to ion  
967 balances in Te cells. (F) Gene sets clusters from GSEA of GO\_MF and GO\_Biological process  
968 (GO\_BP) results in *Nrn1*<sup>-/-</sup> and ctrl Te cells (Figure 4-figure supplement Table 4). (G) Enrichment  
969 of "GOBP\_ membrane repolarization" gene set and enriched gene expression heatmap. (H)  
970 Membrane potential measurement in Te cells. Data represent two independent experiments. (I)  
971 Enrichment of "GOMF\_Metal ion transmembrane transporter activity" gene set and heatmap of  
972 differential gene expression pattern (Figure 4-figure supplement 1B). (J-N) Metabolic changes  
973 associated with *Nrn1*<sup>-/-</sup> Te cell. (J) Enrichment of "GOMF\_ amino acid transmembrane transporter  
974 activity" gene set and differential gene expression heatmap. (K) Phosphorylation of mTOR and  
975 S6 in Te cells measured by flow cytometry. n=3 replicates per group. Data represent two  
976 independent experiments. (L) Measurement of pmTOR and pS6 in Te cells after nutrient sensing.  
977 Data represent three independent experiments. (M) Enriched Hallmark gene sets (p<0.05, FDR  
978 q<0.25). (N) Seahorse analysis of extracellular acidification rate (ECAR) and oxygen consumption  
979 rate (OCR) in *Nrn1*<sup>-/-</sup> and ctrl Te cells. n $\geq$ 6 technical replicates per group. Data represent three  
980 independent experiments. Error bars indicate  $\pm$ SEM. \*p<0.05, \*\*p<0.01, \*\*\*p<0.001,  
981 \*\*\*\*p<0.0001, unpaired Student's t-test was performed for two-group comparison.

982

983

984



985  
986

**Figure 5. Nrn1 deficiency exacerbates autoimmune EAE disease.**

987 (A) Aggravated body weight loss and protracted EAE disease in Nrn1<sup>-/-</sup> mice. (B) CD45<sup>+</sup> cell  
988 number in the spinal cord infiltrates. (C) CD4<sup>+</sup> cell number in the spinal cord infiltrates. (D)  
989 Mog<sub>38-49</sub>/IA<sup>b</sup> tetramer staining of spinal cord infiltrating CD4 cells. (E) Foxp3<sup>+</sup> proportion among  
990 CD4<sup>+</sup> cells in spinal cord infiltrates. (F) IFN $\gamma$ <sup>+</sup> and IL17<sup>+</sup> cell proportion among CD4<sup>+</sup> cells in  
991 draining lymph nodes. n $\geq$ 5 mice per group. Data represent three independent experiments. The P  
992 value was calculated by 2way ANOVA for (A). The p-value was calculated by the unpaired student  
993 t-test for (B-F). \*P<0.05, \*\*P<0.01.

994